

24 Abstract

25 During clathrin-mediated endocytosis in eukaryotes, actin assembly is required to
26 overcome large membrane tension and turgor pressure. However, the molecular
27 mechanisms by which the actin machinery adapts to varying membrane tension
28 remain unknown. In addition, how cells reduce their membrane tension when they
29 are challenged by hypotonic shocks remains unclear. We used quantitative
30 microscopy to demonstrate that cells rapidly reduce their membrane tension using
31 three parallel mechanisms. In addition to using their cell wall for mechanical
32 protection, yeast cells disassemble eisosomes to buffer moderate changes in
33 membrane tension on a minute time scale. Meanwhile, a temporary reduction of the
34 rate of endocytosis for 2 to 6 minutes, and an increase in the rate of exocytosis for at
35 least 5 minutes allow cells to add large pools of membrane to the plasma membrane.
36 We built on these results to submit the cells to abrupt increases in membrane tension
37 and determine that the endocytic actin machinery of fission yeast cells rapidly adapts
38 to perform clathrin-mediated endocytosis. Our study sheds light on the tight
39 connection between membrane tension regulation, endocytosis and exocytosis.

40
41

42 Introduction

43 During clathrin-mediated-endocytosis (CME), the cell plasma membrane
44 undergoes a dramatic change in topology to form an invagination that is
45 subsequently pinched off into a vesicle. During this process, the endocytic machinery
46 has to overcome the forces produced by membrane tension and the osmotic
47 pressure that oppose membrane deformation and engulfment. In yeast cells, these
48 resisting forces are particularly large because their internal turgor pressure is high,
49 ranging from ~0.6 MPa for *Saccharomyces cerevisiae* to more than 1 MPa for
50 *Schizosaccharomyces pombe* (Davi et al., 2018; Minc et al., 2009; Schaber et al.,
51 2010). Consequently the formation of a vesicle requires several thousands of pN
52 (Dmitrieff and Nédélec, 2015; Ma and Berro, 2021).

53 Previous studies have shown that actin dynamics is required for productive
54 endocytosis in yeast (Aghamohammadzadeh et al., 2014; Basu et al., 2013; Carlsson
55 and Bayly, 2014; Palmer et al., 2015) and in mammalian cells when membrane
56 tension is high (Aghamohammadzadeh and Ayscough, 2009; Boulant et al., 2011;
57 Hassinger et al., 2017), or when membrane scission proteins are absent (Ferguson
58 et al., 2009). Actin assembly at the endocytic site is believed to provide the forces
59 that overcome turgor pressure and membrane tension to deform the plasma
60 membrane, but the precise mechanisms of force production remain unknown
61 (reviewed in Berro and Lacy, 2018; Goode et al., 2015; Lacy et al., 2018). We also
62 lack a quantitative understanding of the regulation of actin dynamics in response to
63 membrane tension and turgor pressure changes. We expect that a better quantitative
64 characterization of this response will allow us to infer the molecular mechanisms of
65 force production and force sensing during clathrin-mediated endocytosis.

66 The mechanisms by which membrane tension is regulated are not fully
67 understood. The yeast cell wall is believed to buffer abrupt changes in turgor
68 pressure thanks to its high stiffness of ~50 MPa (Atilgan et al., 2015). In addition,
69 similarly to mammalian cells' caveolae which change shape or disassemble in

70 response to increased membrane tension, yeast eisosomes can also disassemble
71 when cells without a cell wall, called protoplasts, are placed in low osmolarity media
72 (Kabeche et al., 2015; Parton et al., 2019; Sinha et al., 2011). However, it remains
73 unknown how eisosomes may regulate plasma membrane tension in intact cells, and
74 whether eisosome disassembly directly influences cellular processes such as CME.
75 In addition, it remains unclear to which extent endocytosis and exocytosis may
76 contribute to the regulation of membrane tension when the cells are challenged with
77 an abrupt increase in membrane tension.

78 Fission yeast is an ideal model system to quantitatively study the regulation
79 mechanisms of membrane tension and its influence on the endocytic machinery.
80 First, because yeast turgor pressure is high, actin is required for CME. Second,
81 contrary to mammalian cells, yeast cells are devoid of any adhesion machinery or
82 actin cortex, which usually complicates membrane tension manipulation and result
83 interpretation. Last, quantitative microscopy methods developed in fission yeast are
84 able to uncover fine regulations of the endocytic machinery and precisely measure
85 the local and global numbers of endocytic events at a given time (Arasada and
86 Pollard, 2011; Berro et al., 2010; Berro and Lacy, 2018; Berro and Pollard, 2014a,
87 2014b; Chen and Pollard, 2013; Lacy et al., 2019; Sirotkin et al., 2010).

88 To probe the contributions of each possible mechanism of membrane tension
89 regulation and their influence on CME, we submitted yeast cells with or without a cell
90 wall to different hypotonic shocks. Using quantitative fluorescence microscopy, we
91 showed that, on the one hand, yeast cells rapidly reduce their membrane tension by
92 a) disassembling eisosomes, b) reducing their rate of endocytosis and c) increasing
93 their rate of exocytosis, and, on the other hand, actin assembly adapts to increased
94 membrane tension to allow endocytosis to proceed.

95 Results

96 **Eisosomes participate in the regulation of protoplasts' membrane tension**

97 Previous studies proposed that eisosomes, furrows at the inner surface of the
98 plasma membrane, have a mechanoprotective role under increased membrane
99 tension in fungi by acting as a reservoir of membrane, similar to the protective role of
100 caveolae in endothelial cells (Cheng et al., 2015; Kabeche et al., 2015; Lo et al.,
101 2016; Sens and Turner, 2006; Sinha et al., 2011). Since the yeast cell wall plays a
102 major role in the maintenance of cell integrity under extreme osmotic conditions,
103 thanks to its high stiffness of ~50 MPa (Atilgan et al., 2015), it prevents large
104 variations in membrane tension under hypotonic shocks. Hence, to exclude the effect
105 of the cell wall and amplify membrane tension changes, we performed our
106 experiments using cells devoid of a cell wall, hereafter referred to as “protoplasts”,
107 instead of intact cells, hereafter referred to as “walled cells”

108 First, we characterized how the removal of the cell wall affects eisosomes'
109 reorganization. We used a protocol that allowed us to manipulate protoplasts for up
110 to ~1 hour after their formation, since they remain void of cell wall for about 3 hours
111 (Flor-Parra et al., 2014). Because protoplasts are more fragile than walled cells, they
112 were prepared in Edinburgh Minimum Media (EMM5S) containing 0.25 to 1.2 M
113 sorbitol to balance turgor pressure and prevent cells from bursting, while keeping
114 nutrient concentration constant (Basu et al., 2013; Kabeche et al., 2015; Stachowiak
115 et al., 2014), and were imaged ~15 minutes later, once they reached steady state. In
116 the rest of the paper, we will refer to this experimental condition as “steady state in X
117 M” or “chronic exposure to X M sorbitol”, where X is the sorbitol concentration.

118 Our data show that eisosomes in protoplasts at steady state in 1.2 M sorbitol are
119 qualitatively similar to those in walled cells (Figure 1A) and the cellular concentration
120 of Pi1lp is the same in both conditions (Figure 1E). However, the surface area of the
121 protoplasts' plasma membrane covered by eisosomes decreased with decreasing
122 media osmolarity at steady state (Figures 1B and 1C) and correlated with increasing
123 cell volume (Figure 1D). This result confirms previous results (Kabeche et al., 2015)
124 showing that eisosomes are disassembled in media with low osmolarity and the
125 disassembly of eisosomes may reduce membrane tension.

126 We then performed hypotonic shocks to abruptly increase the membrane tension
127 of protoplasts and we imaged them before their long-term adaptation to changes in
128 media osmolarity. Prior to the shocks, we let cells reach steady state by exposing
129 them to media with a given sorbitol concentrations for more than 15 minutes. We
130 chose 0.4 M sorbitol as the steady state concentration for this experiment as it
131 corresponds to the estimated turgor pressure of walled cells (~1 MPa) and at this
132 concentration the dynamics of the actin endocytic machinery was virtually identical to
133 the one in walled cells (Figure 7 – Supplement 1B). We performed acute hypotonic
134 shocks by using a microfluidic system to rapidly exchange the steady state media
135 with media containing a lower sorbitol concentration, hereafter noted $\Delta C = -Y$ M where
136 Y is the difference in media osmolarity (note that the change in pressure ΔP in Pascal
137 is related to the change in osmolite concentration ΔC in Molar as $\Delta P = \Delta C \cdot$
138 $RT \sim 2.45 \cdot 10^6 \cdot \Delta C$, where R is the gas constant and T the absolute temperature,
139 when the solute concentration is sufficiently low).

140 To quantitatively characterize eisosome disassembly in protoplasts after a
141 hypotonic treatment, we measured the temporal evolution of the decrease in surface
142 area covered by eisosomes after an acute hypotonic shock of $\Delta C = -0.2$ M starting

143 with protoplasts at steady state in 0.4 M sorbitol (Figure 1H and 1I). Eisosomes
144 disassembled rapidly after hypotonic shock, dropping to ~50% of the surface area
145 covered by eisosomes before the shock within 5 min, indicating a fast response to
146 counteract the hypotonic shock and an eventual change in membrane tension.

147 To test whether membrane tension is buffered by eisosomes, we measured
148 membrane tension using a micropipette aspiration assay (Figure 1F). At steady state
149 in 0.8 M sorbitol, the membrane tension was 0.45 ± 0.14 mN·m⁻¹ for wild-type
150 protoplasts and 0.39 ± 0.13 mN·m⁻¹ for *pil1Δ* protoplasts (Figure 1G). We then
151 repeated these measurements within 5 minutes after inducing a hypotonic shock of
152 $\Delta C = -0.2$ M. We observed a 1.6-fold increase in membrane tension for wild-type
153 protoplasts (0.73 ± 0.21 mN·m⁻¹) and a 4.5-fold increase for protoplasts lacking
154 eisosomes (1.74 ± 0.61 mN·m⁻¹). This result demonstrates that eisosomes participate
155 in the adjustment of plasma membrane tension.

156

157 **In protoplasts, eisosomes buffer moderate hypotonic shocks**

158 Since WT protoplasts were able to withstand osmotic shocks by disassembling
159 their eisosomes, we hypothesized that protoplasts lacking eisosomes – either
160 because they lack the core eisosome protein Pil1p or because eisosomes are
161 mechanically removed – are more sensitive to hypotonic shocks.

162 WT and *pil1Δ* protoplasts initially at steady state in 0.4 M sorbitol survived small
163 hypotonic shocks ($\Delta C = 0.05$ M) equally well (Figure 2A). However, *pil1Δ* protoplasts
164 were more sensitive to moderate hypotonic shocks ($\Delta C = 0.1$ M) since most of them
165 were unable to survive two minutes after the moderate shock while virtually all the
166 WT protoplasts were able to survive (Figure 2B, Figure 2 – Supplement 1).

167 Moreover, eisosomes were unable to protect protoplasts from larger hypotonic
168 shocks ($\Delta C = 0.2$ M), where most eisosomes are disassembled (Figures 1H and 1I)
169 since most wild-type protoplasts were unable to survive longer than 4 minutes after
170 these high hypotonic shocks, similarly to *pil1Δ* protoplasts (Figure 2C). To further
171 confirm increased death rate was due to the lack of eisosomes, we performed a
172 moderate shock ($\Delta C = 0.1$ M) on protoplasts originally at steady-state in 0.25 M
173 sorbitol where eisosomes are mostly disassembled already. Under these conditions,
174 WT protoplasts survival was comparable to the survival of *pil1Δ* (Figure 2D). This
175 result further demonstrates that the presence of assembled eisosomes at the plasma
176 membrane is indeed responsible for the adaptation of cells to acute hypotonic
177 shocks, and the presence of Pil1p in the cytoplasm is not sufficient for this response.

178 Altogether, these experiments demonstrate that a) eisosomes protect protoplasts
179 from changes in their membrane tension, but only to a small extent, b) without
180 eisosomes, protoplasts can withstand only minor increase in their membrane tension.

181

182 **Eisosomes protect the integrity of walled cells during consecutive osmotic shocks**

183

184 We observed that a significant number of both wild-type and *pil1Δ* protoplasts
185 died after osmotic shocks, and the percentage of *pil1Δ* protoplasts that remained
186 alive was significantly smaller than for wild-type protoplasts even under moderate
187 shocks ΔC of -0.05 M, -0.1 M and -0.2 M (Figures 2A-C). In contrast, we found that
188 both wild-type and *pil1Δ* walled cells can survive a single osmotic shock of $\Delta C = -1.2$
189 M, which initially led us to think that eisosomes only have a minor protective role in
190 walled cells (Figure 2F). However, we noticed that subsequent osmotic shocks led to
191 a higher mortality of *pil1Δ* compare to wild-type walled cells. While almost all the wild-
192 type walled cells remained alive after several shocks, around 10% of *pil1Δ* walled

193 cells died after each subsequent shock (Figures 2E,2F and 2G; supplementary video
194 1 and 2). These results demonstrate that, even in walled cells, eisosomes exert a
195 protective role, likely by buffering sudden changes in membrane tension.

196

197 **Membrane tension and eisosomes modulate the rate of endocytosis in cells**

198 Within a few minutes of a hypotonic shock, the volume of WT protoplasts
199 increased up to 50% and the volume of *pil1Δ* protoplasts increased up to 20%
200 (Figures 3A and 3B, insets). However, the corresponding increase in surface area
201 cannot be explained by eisosome disassembly alone – total eisosome disassembly
202 could release about 5% of the total surface area of the plasma membrane, assuming
203 eisosomes are hemi-cylinders with diameter ~50 nm and cells contain 1.6 μm of
204 eisosomes per μm^2 of plasma membrane on average (Kabeche et al., 2015).
205 Therefore, another mechanism for protoplasts to gain plasma membrane occurs in
206 the first few minutes after hypotonic shocks. We hypothesized that a decrease in the
207 number of endocytic events happening in the cell after a hypotonic shock would
208 gradually increase the surface area of the plasma membrane and reduce membrane
209 tension.

210 We measured the endocytic density, i.e. the number of endocytic events in a cell
211 normalized by the cell length, in wild-type and *pil1Δ* cells after a hypotonic shock
212 using a ratiometric method (Berro and Pollard, 2014a). In brief, this method consists
213 of imaging cells expressing a fluorescently tagged endocytic protein, here the actin
214 filament crosslinking protein fimbrin (Fim1p) tagged with a monomeric enhanced
215 green fluorescent protein (mEGFP), hereafter called Fim1p-mEGFP. First, we
216 measure the temporal average intensity of the fluorescent protein at endocytic sites.
217 Second, we measure the whole intensity of each cells from which the corresponding
218 cytoplasmic intensity is subtracted – this number represents the sum of the
219 intensities for all the fluorescently tagged proteins present at endocytic sites. The
220 number of endocytic sites in each cell is then calculated as the ratio between those
221 two numbers. The endocytic density is calculated by dividing this ratio with the cell
222 length.

223 For all shocks tested in wild-type ($\Delta\text{C}=-0.05$ M, -0.1 M, -0.2 M) and *pil1Δ*
224 protoplasts ($\Delta\text{C}=-0.025$ M, -0.05 M, -0.1 M) initially at steady state in 0.4 M sorbitol,
225 the endocytic density in protoplasts significantly decreased immediately after the
226 hypotonic shock (Figure 3A). The difference increased for increasing hypotonic
227 shocks, up to 36% for wild-type protoplasts after a $\Delta\text{C}=-0.2$ M shock, and 79% for
228 *pil1Δ* protoplasts after a $\Delta\text{C}=-0.1$ M shock (Figure 3B). These abrupt changes in the
229 endocytic density were followed by a 2- to 6-minute recovery back to the steady-state
230 endocytic density, and recovery time depended on the magnitude of the hypotonic
231 shock. Note that the change in cell volume (Figures 3A and 3B, insets) could not
232 exclusively account for the observed decrease in the endocytic density in wild-type
233 cells as the relative increase in cell volumes were larger than the relative decrease in
234 endocytic density 2 minutes after the shocks and remained large 4 minutes after
235 while the endocytic densities recovered their pre-shock values.

236 Building on these results in protoplasts, we wondered whether the endocytic
237 density in walled cells also adapts to hypotonic shocks. Indeed, immediately after the
238 largest shock tested ($\Delta\text{C}=-1.2$ M), we observed a similar decrease in the endocytic
239 density for both wild-type and *pil1Δ* walled cells, 36% and 46% respectively (Figure
240 3D). Recovery to steady-state endocytic densities occurred in less than 2 minutes in
241 both wild-type and *pil1Δ* walled cells, faster than in protoplasts (Figures 3A, 3B and

242 3D). Our data show that the cell wall limits but does not completely cancel the effect
243 of hypotonic shocks on endocytic rates. They also suggest that the regulation of the
244 endocytic density supplements the regulation performed by the eisosomes to reduce
245 membrane tension.

246 Wild-type and *pil1Δ* walled cells had a very similar adaptation after hypotonic
247 shocks. However, we noticed a difference in the endocytic density at steady state in
248 different sorbitol concentrations. For all concentrations tested (0 to 2 M), wild-type
249 cells maintained roughly the same endocytic density. In contrast, the steady state
250 endocytic density in *pil1Δ* cells increased with increasing media osmolarity, up to
251 56% in 2 M sorbitol (Figure 3C). Our results suggest that eisosomes participate in
252 maintaining a constant density of endocytosis independently of the media osmolarity,
253 not only after an abrupt change in membrane tension, but also when they are at
254 steady state in different osmolarity.

255

256 **The exocytosis rate increases after a hypotonic shock in protoplasts but not in** 257 **walled cells**

258 Reciprocal to the decrease in the number of endocytic events observed after a
259 hypotonic shock, we wondered whether the rate of exocytosis increases in the
260 meantime to provide more surface area to the plasma membrane, as has been
261 observed in mammalian cells (Gauthier et al., 2009).

262 To measure the rate of exocytosis in different conditions, we used the cell
263 impermeable styryl dye FM4-64, whose fluorescence dramatically increases when it
264 binds to membranes (Cochilla et al., 1999; Gachet and Hyams, 2005; Richards et al.,
265 2000). After FM4-64 is introduced to the media, the plasma membrane is rapidly
266 stained (Figure 4A). Fusion of unstained intracellular vesicles to the plasma
267 membrane results in an increase of total cell fluorescence, because after each fusion
268 event new unstained membrane from the interior of the cell is exposed to the dye. At
269 this stage, if one wanted to measure endocytosis rates, one would typically remove
270 the FM4-64 dye from the media to destain the plasma membrane, and quantify the
271 internal fluorescence which is proportional to the amount of membrane internalized
272 by endocytosis. Here, we kept the FM4-64 dye in the media, and monitored the
273 fluorescence of the plasma membrane and the interior of the cell. In this case,
274 endocytic events do not increase the total cell fluorescence because they transfer
275 patches of the plasma membrane that are already stained into the interior of the cell
276 (Figure 4A, red arrow). Therefore, the increase in fluorescence we measured is due
277 to the addition of new unstained lipids to the plasma membrane by exocytosis (Figure
278 4A, gray arrow). Note that the increase in total cell fluorescence could also be due to
279 putative transfer of lipids by non-exocytic mechanisms (Reinisch and Prinz, 2021) but
280 for simplicity and by lack of further evidence, onwards we will interpret the increase in
281 fluorescence to an increase in the exocytosis rate.

282 Staining of wild-type fission yeast with 20 μ M FM4-64 in EMM5S (Figure 4B)
283 showed that after a brief phase of rapid staining of the cell surface, the total cell
284 fluorescence intensity grows roughly linearly for at least 20 minutes, and the slope of
285 the normalized intensity corresponds to the exocytosis rate as a percentage of the
286 plasma membrane surface area per unit of time (see materials and methods)
287 (Gauthier et al., 2009; Smith and Betz, 1996; Vida and Emr, 1995). Using this
288 method, we measured that wild-type walled cells at steady state in EMM5S
289 exocytose 4.6% of their plasma membrane surface area per minute (Figure 4B).
290 FM4-64 staining did not seem to affect the endocytic and exocytic membrane

291 trafficking of yeast cells, since stained vesicles are successfully released after
292 washing cells with fresh media (Figure 4B).

293 We measured the exocytosis rates in the conditions that had the largest
294 effects on the rates of endocytosis while keeping most cells alive, i.e. we used
295 protoplasts at steady state in 0.4 M and performed a $\Delta C = -0.2$ M shock for wild-type
296 and $\Delta C = -0.05$ M shock for *pil1Δ*. At steady state in 0.4M sorbitol (Figures 4F and
297 4H), wild-type protoplasts had an exocytosis rate similar to walled cells in EMM5S in
298 0 M ($k_{0.5} = 4.4 \pm 0.2\% \text{ min}^{-1}$). After a $\Delta C = -0.2$ M shock, the exocytosis rate increased by
299 41% ($k_{0.5} = 6.2 \pm 0.4\% \text{ min}^{-1}$). At steady state in 0.4 M sorbitol (Figures 4G and 4H), the
300 exocytosis rate of *pil1Δ* protoplasts was higher than for walled cells in 0 M sorbitol
301 ($k_{0.5} = 6.2 \pm 0.4\% \text{ min}^{-1}$). After a $\Delta C = -0.05$ M shock, the exocytosis rate increased
302 modestly ($k_{0.5} = 6.8 \pm 0.5\% \text{ min}^{-1}$). Therefore, in both wild-type and *pil1Δ* protoplasts, an
303 acute hypotonic shock leads to an increased exocytosis rate, which increases
304 surface area and likely reduces membrane tension. The change in exocytosis rate in
305 *pil1Δ* protoplasts being more modest than in wild-type cells highlights the role of
306 eisosomes in buffering the change in the exocytosis rate in response to change in
307 osmolarity and membrane tension.

308 We wondered whether these changes in exocytosis rate also happen in walled
309 cells. First, we measured exocytosis rate at steady state in solutions with different
310 molarities and found that the rates were smaller than in protoplasts (Figures 4C-E).
311 The exocytosis rate of wild-type walled cells at steady state in 1.2M sorbitol ($k_{0.5}$
312 $= 3.1 \pm 0.1\% \text{ min}^{-1}$, Figures 4C and 4E) was 35% smaller than in 0 M sorbitol ($k_{0.5}$
313 $= 4.8 \pm 0.1\% \text{ min}^{-1}$, Figure 4B). In addition, in *pil1Δ* walled cells, the exocytosis rate of
314 walled cells lacking eisosomes in 1.2M sorbitol was only slightly smaller than wild-
315 type cells in the same conditions ($k_{0.5} = 2.6 \pm 0.1\% \text{ min}^{-1}$, Figures 4D and 4E). After
316 hypotonic shocks, the change of exocytosis rate in walled cells was very limited
317 (Figures 4C-E). In fact, our strongest hypotonic shock of $\Delta C = -1.2$ M did not
318 significantly increase the exocytosis rate of wild-type or *pil1Δ* cells walled cells
319 (Figure 4E). These data corroborate our previous finding that the cell wall limits but
320 does not completely cancel the effect of hypotonic shocks in intact cells. In addition,
321 they also demonstrate that eisosomes are involved in the regulation of the exocytosis
322 rate.

323

324 **Inhibition of exocytosis decreased the survival rate of protoplasts under acute** 325 **hypotonic shock and inhibition of endocytosis increased their survival rate**

326 To further test our hypothesis that reducing the endocytosis rate and
327 increasing the exocytosis rate help regulate membrane tension after a hypotonic
328 shock, we blocked endocytosis or exocytosis with drugs and measured the survival
329 rates of cells. We hypothesized that inhibition of endocytosis or exocytosis would
330 have opposite effects on the survival of protoplasts under acute hypotonic shock.
331 Specifically, inhibition of endocytosis would help retain membrane on the surface of
332 protoplasts, thereby reducing the probability of membrane rupture. Conversely,
333 inhibition of exocytosis would reduce the transfer of membrane from intracellular
334 vesicles to the surface of protoplasts, exacerbating the lack of plasma membrane in
335 the face of imminent protoplast expansion. To observe the largest effects, we used
336 *pil1Δ* protoplasts under $\Delta C = -0.2$ M shock and exposed the cells to either Latrunculin
337 A (LatA) or Brefeldin A (BFA) for 30 minutes before the shocks.

338 Blocking exocytosis with BFA increased the death rate of protoplasts after
339 hypotonic shocks, confirming our hypothesis (Figure 5). Blocking actin assembly, and

340 therefore endocytosis, with LatA made the protoplasts more resistant starting 4
341 minutes after the hypotonic shock, also confirming our hypothesis. Note that LatA
342 treatment made the protoplasts less resistant to shock in the initial 2 minutes after
343 the hypotonic shock, which seems in contradiction with our hypothesis. However, it is
344 possible that prolonged treatment with LatA had other unidentified effects on
345 protoplasts survival or may indirectly affect the exocytosis rate since LatA affects all
346 actin structures in the cell, including actin cables which are needed for the transport
347 of exocytic vesicles (Lo Presti et al., 2012).

348

349 **Actin dynamics during clathrin-mediated endocytosis in wild-type walled cells** 350 **is robust over a wide range of chronic and acute changes in media osmolarity**

351 Next, we wondered how the actin machinery adapts to different changes in
352 osmotic pressure and membrane tension. To monitor actin dynamics during clathrin-
353 mediated endocytosis, we imaged fission yeast cells expressing Fim1p-mEGFP
354 (Figures 6A and 6B). Fimbrin is a bona fide marker for endocytosis in yeast since it
355 has spatial and temporal co-localization with the classical endocytic marker End4p
356 (the fission yeast homolog of mammalian Hip1R and budding yeast Sla2) during
357 endocytosis (Figure 6 – Supplement 1A and 6 – Supplement 1B). Fimbrin's time of
358 appearance, disappearance, peak number of molecules and spatial localization
359 follows those of actin in wild-type cells and all mutants tested so far (Arasada et al.,
360 2018; Berro and Pollard, 2014b; Chen and Pollard, 2013; Sirotkin et al., 2010).
361 Fimbrin is the most abundant endocytic proteins that is fully functional when tagged
362 with a fluorescent protein at either N- or C-terminal. Tagged fimbrin is a more robust
363 marker for actin dynamics than tagged actin or actin-binding markers such as LifeAct
364 or calponin-homology domains, because they require over-expression which is
365 difficult to control precisely in fission yeast, and potentially creates artifacts
366 (Courtemanche et al., 2016; Suarez et al., 2015). Fimbrin is also a central player in
367 force production during CME in yeast (Ma and Berro, 2019, 2018; Picco et al., 2018;
368 Planade et al., 2019). We optimized our imaging protocols, and improved tracking
369 tools and temporal super-resolution alignment methods (Berro and Pollard, 2014a) to
370 a) easily collect hundreds of endocytic events in an unbiased manner and b) achieve
371 high reproducibility between different samples, fields of view and days of experiment
372 (Figures 6C and 6 – Supplement 2A). These improvements in our quantitative
373 microscopy protocol have allowed us to detect small differences between mutants or
374 conditions that would be missed with previous methods. We confirmed that Fim1p
375 accumulates at endocytic sites for about 10 seconds, and then disassembles while
376 the vesicle diffuses away from the plasma membrane (Figures 6C and 6 –
377 Supplement 2A) (Sirotkin et al., 2010; Skau et al., 2011). As a convention, the peak
378 number of Fim1p molecules is set to time 0 s and corresponds to vesicle scission in
379 intact wild-type cells (Berro and Pollard, 2014a, 2014b; Sirotkin et al., 2010).

380 For all tested osmolarities at steady state in walled wild-type cells, we observed
381 no significant difference in the dynamics of fimbrin recruitment or disassembly,
382 maximum molecule number or endocytic patch movements (Figure 6D). Our results
383 indicate that wild-type walled cells have adaptation mechanisms for chronic exposure
384 to a wide range of osmolarities, which allows them to perform CME in a highly
385 reproducible manner.

386 We then tested the robustness of the endocytic actin machinery when cells
387 experienced a hypotonic shock, which aimed to abruptly increase the tension of their
388 plasma membrane. To observe the highest possible effect, we imaged cells grown at
389 steady state in 1.2 M sorbitol and rapidly exchanged the media with a buffer free of

390 sorbitol (Figures 6F and 6G), therefore performing an acute hypotonic shock of $\Delta C =$
391 1.2 M. Despite the high hypotonic shock, which represents a ~ 3 MPa drop in
392 pressure, CME proceeded quite similarly to steady state conditions (Figures 6G, 6 –
393 Supplement 3). The maximum number of fimbrin proteins was the same before and
394 after the hypotonic shock, but fimbrin assembly and disassembly were $\sim 15\%$ faster
395 after the shock.

396

397 **Eisosomes mitigate the response of the endocytic machinery to acute and** 398 **chronic changes in media osmolarity**

399 The robustness of the endocytic process under a wide range of chronic and acute
400 exposure to different media osmolarity is consistent with our previous results showing
401 that fission yeast cells rapidly regulate plasma membrane tension. To better
402 understand the role of eisosomes and amplify the change in membrane tension after
403 hypotonic shocks, we repeated our experiments in *pil1 Δ* cells which lack eisosomes
404 (Figure 6E).

405 Dynamics of Fim1p during CME for wild-type and *pil1 Δ* walled cells at steady
406 state in media free of sorbitol were identical (Figure 6 – Supplement 1C). However, at
407 steady state in media with high sorbitol concentration, cells lacking eisosomes
408 recruited slightly fewer fimbrin molecules to endocytic patches than wild-type cells
409 (Figure 6E). The maximum number of Fim1p assembled at CME sites in *pil1 Δ* cells in
410 buffer containing 0.8 M and 1.2 M sorbitol was 10% and 17% lower, respectively.
411 Within the first two minutes of an acute hypotonic shock from 1.2 M sorbitol to 0 M
412 ($\Delta C = -1.2$ M), the maximum number of Fim1p increased by 30%, while its timing was
413 shortened by $\sim 30\%$ compared to steady-state (Figure 6H). Four minutes after the
414 hypotonic shock, the dynamics of fimbrin stabilized at its steady state dynamics in 0
415 M sorbitol (Figures 6E and 6H). Overall, our data show that the endocytic actin
416 machinery in cells lacking eisosomes is more sensitive to acute and chronic changes
417 in media osmolarity than in wild-type cells, consistent with a role for eisosome in
418 regulating membrane tension at endocytic sites.

419

420 **CME in protoplasts is sensitive to chronic changes in osmolarity**

421 Endocytosis in wild-type protoplasts at steady state in medium containing 0.4 or
422 0.8 M sorbitol was able to proceed normally by recruiting almost the same number of
423 fimbrin molecules as in walled cells, but with a slightly longer timing (Figure 7 –
424 Supplement 1B). In contrast, in medium with 1.2 M sorbitol, the timing of fimbrin
425 recruitment was dramatically longer, and endocytosis failed to proceed normally, as
426 reported by the virtually null speed of patches during the entire time fimbrin was
427 present at the endocytic site (Figure 7 – Supplement 1B). Cells lacking eisosomes
428 had very similar phenotypes but endocytosis started failing at 0.8 M sorbitol (Figure 7
429 – Supplement 1C).

430 At 0.25 M sorbitol, both wild-type and *pil1 Δ* protoplasts were able to perform
431 endocytosis but required a larger amount of Fim1p (Figures 7 – Supplements 1B and
432 7 – Supplements 1C). In these conditions, the eisosomes covered only half of the
433 plasma membrane surface area they cover at 0.4M sorbitol (Figures 1B and 1C) and
434 our data suggest the plasma membrane was under high tension (Figure 1G). This
435 result indicates that during CME the actin machinery is able to adapt to mechanical
436 cues by mechanisms that are independent of the cell wall.

437 For both wild-type and *pil1 Δ* protoplasts in 0.4 M sorbitol, the temporal evolution
438 of the number of fimbrin molecules and the speed of patches were close to the same
439 metrics measured in walled cells in media without sorbitol (Figures 7 – Supplements

440 1B and 7 – Supplements 1C). These results suggest that the osmotic pressure at
441 these concentrations, which are equivalent to a pressure of 1 MPa, is close to the
442 naturally maintained turgor pressure of walled fission yeast cells, in good agreement
443 with previous measurements (Minc et al., 2009). Therefore, to keep protoplasts in
444 conditions close to walled cells, the steady state media used in our following
445 experiments on protoplasts contained 0.4 M sorbitol.

446

447 **The endocytic actin machinery rapidly adapts to increases in membrane** 448 **tension**

449 To characterize the adaptation of the endocytic actin machinery to a rapid
450 increase in turgor pressure and membrane tension, we repeated our acute hypotonic
451 shocks ($\Delta C = -0.05$ M, -0.1 M or -0.2 M) on protoplasts initially at steady state in media
452 containing 0.4 M sorbitol. After low ($\Delta C = -0.05$ M) and medium ($\Delta C = -0.1$ M) acute
453 shocks in wild-type protoplasts, we did not observe any stalled endocytic events –
454 when cells started the recruitment of the actin machinery, endocytosis proceeded to
455 successful completion (Figures 7A-C and 7 – Supplement 5). The recruitment of
456 fimbrin did not significantly change over time. In contrast, two minutes after a $\Delta C =$
457 -0.2 M shock, endocytic sites recruited 20% more fimbrin and it took ~25% longer to
458 perform endocytosis (Figures 7C, 7D, and 7 – Supplement 5). The actin machinery
459 restored its steady state behavior less than 4 minutes after the shock (Figure 7D).

460 We repeated these experiments with *pil1* Δ protoplasts to eliminate the role of
461 eisosomes in the reduction of membrane tension during hypotonic shocks.
462 Immediately (0 minute) after the lowest hypotonic shock tested ($\Delta C = -0.05$ M), fimbrin
463 recruitment took slightly longer and the number of proteins recruited was higher than
464 at steady state (Figures 7E-G and 7 – Supplement 6). While fimbrin restored its
465 steady-state dynamics in less than 4 minutes after high acute hypotonic shock ($\Delta C =$
466 -0.2 M) in wild-type protoplasts (Figure 7D), recovery of fimbrin dynamics to its steady
467 state behavior in *pil1* Δ protoplasts occurred over 10 minutes, even for the most
468 modest hypotonic shock, $\Delta C = -0.05$ M (Figure 7G). The changes in fimbrin dynamics
469 in *pil1* Δ protoplasts became increasingly larger for $\Delta C = -0.1$ M and $\Delta C = -0.2$ M
470 hypotonic shocks – endocytic sites assembled a peak number of fimbrin respectively
471 ~25% and ~50% larger and took ~85% and ~50% longer.

472 Wild-type protoplasts at steady state in 0.25 M sorbitol contain significantly fewer
473 assembled eisosomes despite expressing normal amounts of Pil1p (Figures 1B, 1C
474 and 1E). We took advantage of this condition to test whether the absence of
475 eisosomes structures at the plasma membrane and not the absence of the protein
476 Pil1p is responsible for changes in actin dynamics after an acute hypotonic shock.
477 We subjected wild-type protoplasts at steady state in 0.25 M sorbitol to an acute
478 hypotonic shock of $\Delta C = -0.1$ M (Figures 7H and 7I). Two minutes after the shock,
479 endocytic sites accumulated 73% more fimbrin and took ~60% longer (Figures 7H
480 and 7 – Supplement 7A). This behavior was nearly identical to fimbrin dynamics in
481 *pil1* Δ protoplasts under the same conditions (Figure 7I and Figure 7 – Supplement
482 7B).

483 Altogether, these experiments demonstrate that a) the endocytic actin machinery
484 adapts to compensate the increase in membrane tension, and b) actin dynamics
485 restores its steady state behavior within a few minutes, providing the protoplasts
486 survived the hypotonic shock.

487

488 **Discussion**

489 **Mechanisms of tension regulation and homeostasis of the plasma membrane**

490 Our results demonstrate that the regulation of membrane tension in hypotonic
491 environment is performed via a combination of at least three mechanisms: the
492 mechanical protection by the cell wall, the disassembly of eisosomes and the
493 temporary shift in the balance between endocytosis and exocytosis (Figure 8). Our
494 data indicate that all three mechanisms are used in parallel, since wild-type walled
495 cells are less sensitive to acute hypotonic shocks than wild-type protoplasts and
496 *pil1Δ* walled cells, and they experience a temporary decrease in their endocytic
497 density for about 2 minutes after the shock. In addition, our data allow us to estimate
498 the relative contribution of each mechanism in the regulation of membrane tension.

499 The cell wall provides the largest protection during chronic and acute
500 hypotonic shocks. Wild-type walled cells are virtually insensitive to osmotic
501 downshifts, and *pil1Δ* walled cells are much less sensitive than *pil1Δ* protoplasts.
502 Removal of the cell wall dramatically affects actin dynamics at endocytic sites and
503 eisosome assembly at the plasma membrane (Figures 1B, 1C, 7 – Supplement 1B
504 and 7 – Supplement 1C), and greatly increased the effect of hypotonic shock on
505 exocytosis (Figure 4). It is surprising that endocytosis in protoplasts still proceeds in
506 media with osmolarity as low as 0.25 M, where a large fraction of eisosomes is
507 disassembled. In fact, the actin endocytic machinery can overcome membrane
508 tensions high enough to rupture the plasma membrane since we did not see stalled
509 actin patches, or actin comet tails, in any of our experiments. Our results contrast
510 with recent data in *S. cerevisiae* (Riggi et al., 2019) where endocytosis is blocked
511 and actin comet tails are formed within 2 minutes of a hypotonic shock. These
512 differences may highlight species specificities.

513 Our results add to a growing body of evidence that eisosomes play a critical
514 role in the regulation of membrane tension and membrane integrity through dynamic
515 remodeling and scaffolding of the plasma membrane (Kabeche et al., 2015; Moseley,
516 2018). Endocytosis in wild-type walled cells is not sensitive to chronic or acute
517 hypotonic changes, whereas *pil1Δ* walled cells endocytosis is (Figure 6). Conversely,
518 exocytosis seems to respond more strongly to acute hypotonic shock in wild-type
519 walled cells than in *pil1Δ* walled cells (Figure 4). The protective role of eisosomes is
520 even more striking in protoplasts under acute hypotonic shocks. Wild-type
521 protoplasts whose plasma membrane is covered with eisosomes are largely
522 insensitive to increases in membrane tension whereas protoplasts with little to no
523 eisosomes are extremely sensitive to increases in membrane tension and their
524 plasma membrane is easily damaged (Figures 2A-C). Eisosomes retain this
525 protective function even in walled cells, which becomes evident when cells are put
526 under repeated osmolarity shocks (Figures 2E-G). Our micropipette aspiration
527 experiments also demonstrate that eisosomes are critical to keep membrane tension
528 low during an acute hypotonic shock. Therefore, our data indicate that membrane
529 tension is decreased via the disassembly of eisosomes, through release of excess
530 membrane surface area. Assuming eisosomes are hemi-cylinders with diameter ~50
531 nm and cells contain 1.6 μm of eisosomes per μm^2 of plasma membrane on average,
532 total eisosome disassembly could release about 5% of the total surface area of the
533 plasma membrane over ~3 minutes after a hypotonic shock (Kabeche et al., 2015),
534 although a mild shock of $\Delta C = -0.2$ M disassembled close to ~50% eisosomes over 5
535 minutes, or about 2.5% of the surface area of the plasma membrane (Figures 1H and
536 1I). Single-molecule imaging in our lab demonstrated that at steady state Pil1p
537 undergoes rapid exchange at the eisosome ends (Lacy et al., 2017), potentially
538 providing a convenient route for rapid eisosome disassembly, analogous to filament

539 depolymerization, in combination with eisosome breaking. Disassembled eisosome
540 components have altered phosphorylation level or sub-cellular localization, which
541 potentially relays the signaling from eisosome integrity to endocytosis and/or
542 exocytosis (Riggi et al., 2018; Walther et al., 2007), possibly via TORC2 (Riggi et al.,
543 2019).

544 Our study highlights a third mechanism to reduce membrane tension by
545 increasing the surface area of the plasma membrane via a temporary reduction in the
546 endocytosis rate and an increase in the exocytosis rate. Using our data, we estimate
547 that cells endocytose about 2% of their surface area per minute through clathrin
548 mediated endocytosis, confirming our previous measurements (Berro and Pollard,
549 2014a, 2014b). During acute hypotonic shock, a reduction of the endocytosis rate
550 plus an increase in the exocytosis rate for a few minutes would allow for a net
551 addition of surface area to the plasma membrane. For example, in *pil1Δ* protoplasts
552 initially at steady state in 0.4 M sorbitol the endocytosis rate is reduced by ~25 % for
553 ~10 minutes after an acute hypotonic shock of $\Delta C = -0.05$ M, while the exocytosis rate
554 increased by ~10%. The net surface area added over that period by reduction in
555 endocytosis and increase in exocytosis corresponds to a 5% + 6% = 11% increase in
556 the protoplast surface area, close to the ~12% surface area increase we measured.
557 These results confirm and quantify previous reports of control of surface tension by
558 increasing the surface area via a modulation of endocytosis and exocytosis rates in
559 other eukaryotes (Apodaca, 2002; Homann, 1998; Morris and Homann, 2001). These
560 estimates demonstrate that modulating the endocytosis and exocytosis rates is an
561 efficient way to increase the surface area of the plasma membrane by large amounts,
562 but this process is relatively slow compared to eisosome disassembly. The slowness
563 of this process might explain why *pil1Δ* and pre-stretched wild-type protoplasts that
564 have about half the normal amount of eisosomes on their surface do not survive even
565 relatively small hypotonic shocks, being unable to provide enough membrane in a
566 short amount of time to reduce the tension of their plasma membrane.

567 For the calculations presented above, we have assumed that the size of
568 endocytic and exocytic vesicles remain constant in all osmotic conditions. However,
569 further experiments will be necessary to validate or invalidate this assumption. In
570 addition, our FM4-64 data does not allow us to distinguish between lipid addition to
571 the plasma membrane via exocytosis or via a putative transfer of lipids by non-
572 exocytic mechanisms (Reinisch and Prinz, 2021) and for simplicity and by lack of
573 further evidence, we have discussed our data as an increase in the exocytosis rate.
574 Not much is known about lipid transfer proteins at the plasma membrane and further
575 experiments will be necessary to determine whether the activity of these proteins is
576 enhanced by abrupt increases in membrane tension or hypotonic shocks.

577 578 **Molecular mechanisms driving the adaptation of the actin endocytic machinery** 579 **and the rate of endocytosis under various membrane tensions**

580 Our data demonstrate that fission yeast CME is very robust and can proceed
581 in a wide range of osmolarities and membrane tension. Even cells devoid of a cell
582 wall and eisosomes were able to perform endocytosis after an acute change in
583 membrane tension, as long as their plasma membrane was not damaged and cells
584 remained alive. Even in the most extreme conditions tested, i.e. cells devoid of a cell
585 wall and lacking the majority of their eisosomes, the peak number of molecules and
586 timing of fimbrin at endocytic sites was only two times larger than what was observed
587 in wild-type walled cells.

588 Under conditions where membrane tension and turgor pressure were
589 significantly increased, we observed that the endocytic actin machinery took longer
590 and assembled a larger number of fimbrin molecules to successfully produce
591 endocytic vesicles. This effect increased with increasing membrane tension, up to
592 tensions high enough to rupture the cell plasma membrane. This result strongly
593 supports the idea that the actin machinery provides the force that counteracts
594 membrane tension and turgor pressure and deforms the plasma membrane into an
595 endocytic pit.

596 The precise molecular mechanism that regulates this enhanced assembly
597 remains to be uncovered. Our data suggest that actin dynamics is controlled via a
598 mechanical or geometrical regulation, where actin assembles until the plasma
599 membrane is deformed and pinched off. An alternative, and non-mutually exclusive,
600 hypothesis is that the activity and/or recruitment of proteins upstream of the actin
601 nucleators may be enhanced by increased membrane tension. A third hypothesis is
602 that the decrease in the number of endocytic events after an increase in membrane
603 tension leads to an increase in the concentration of endocytic proteins in the
604 cytoplasm, which can then enhance the reactions performed at the endocytic sites.
605 Sirotkin et al (Sirotkin et al., 2010) measured that 65% to 85% of the total cellular
606 content of key proteins involved in the endocytic actin machinery are localized to
607 endocytic sites at any time. A 20% decrease in the number of endocytic sites would
608 increase their cytoplasmic abundance by roughly 40% to 80%. This percentage is
609 larger than the volume changes we measured, resulting in a net increase in the
610 cytoplasmic concentration of these proteins, which would allow larger amount of
611 protein to assemble at the endocytic sites.

612 Conversely, the decreased endocytosis rate could be attributed to the larger
613 number of endocytic proteins assembled at each endocytic site, which would
614 decrease their cytoplasmic concentration. Indeed, Burke *et al.* (Burke et al., 2014)
615 showed that modulating actin concentration modulates the number of endocytic sites
616 in the same direction. However, it is more likely that one or several early endocytic
617 proteins are sensitive to membrane tension, and either fail to bind the plasma
618 membrane or prevent the triggering of actin assembly when membrane tension is
619 high. This idea would be consistent with results from mammalian cells demonstrating
620 that the proportion of stalled clathrin-coated pits increases when membrane tension
621 increases (Ferguson et al., 2017). In addition, several endocytic proteins that arrive
622 before or concomitantly with the activators of the actin machinery contain BAR
623 domains (such as Syp1p, Bzz1p and Cdc15p), and other members of this domain
624 family (which also includes Pil1p) have been shown to bind membranes in a tension-
625 sensitive manner. Further quantitative study of early endocytic proteins will help
626 uncover the validity and relative contributions of each one of these hypotheses.

627 We expect our results to be relevant to the study of CME and membrane
628 tension regulation in other eukaryotes since the molecular machineries for
629 endocytosis, exocytosis and osmotic response are highly conserved. In addition,
630 regulation of membrane tension and CME are particularly critical during cell
631 polarization (Mostov et al., 2000), during neuron development and shape changes
632 (Urbina et al., 2018) and at synapses where large pools of membranes are added
633 and retrieved on a very fast time scale (Nicholson-Fish et al., 2016; Watanabe and
634 Boucrot, 2017).

635

636 **Materials and Methods**

637 **Yeast strains and media**

638 The *S. pombe* strains used in this study are listed in Supplemental Table S1.
639 Yeast cells were grown in YE5S (Yeast Extract supplemented with 0.225 g/L of
640 uracil, lysine, histidine, adenine and leucine), which was supplemented with 0 to 1.2
641 M D-Sorbitol, at 32°C in exponential phase for about 18 hours. Cells were washed
642 twice and resuspended in filtered EMM5S (Edinburgh Minimum media supplemented
643 with 0.225 g/L of uracil, lysine, histidine, adenine and leucine), which was
644 supplemented with the same concentration of D-Sorbitol, at least 10 minutes before
645 imaging so they can adapt and reach steady state.

646 **Protoplasts preparation**

647 *S. pombe* cells were grown in YE5S at 32°C in exponential phase for about 18
648 hours. 10 mL of cells were harvested and washed two times with SCS buffer (20 mM
649 citrate buffer, 1 M D-Sorbitol, pH=5.8), and resuspended in SCS supplemented with
650 0.1 g/mL Lallzyme (Lallemand, Montreal, Canada) (Flor-Parra et al., 2014). Cells
651 were incubated with gentle shaking for 10 minutes at 37°C in the dark except for
652 experiments in Figure 5, where cells were digested at room temperature with gentle
653 shaking for 30 minutes in the presence of inhibitors. The resulting protoplasts were
654 gently washed twice in EMM5S with 0.25 to 1.2 M D-Sorbitol, spun down for 3
655 minutes at 960 rcf between washes, and resuspended in EMM5S buffer
656 supplemented with 0.25 to 1.2 M D-Sorbitol at least 10 minutes before imaging so
657 they can adapt and reach steady state.
658
659

660 **Microscopy**

661 Microscopy was performed using a spinning disk confocal microscope, built on
662 a TiE inverted microscope (Nikon, Tokyo, Japan), equipped with a CSU-W1 spinning
663 head (Yokogawa Electric Corporation, Tokyo, Japan), a 100X/1.45NA Phase
664 objective, an iXon Ultra888 EMCCD camera (Andor, Belfast, UK), and the NIS-
665 Elements software v. 4.30.02 (Nikon, Tokyo, Japan) on. The full system was
666 switched on at least 45 minutes prior to any experiments to stabilize the laser power
667 and the room temperature. Cells were loaded into commercially available
668 microfluidics chambers for haploid yeast cells (Y04C-02-5PK, Millipore-Sigma, Saint-
669 Louis, USA) for the CellASIC ONIX2 microfluidics system (Millipore-Sigma, Saint-
670 Louis, USA). Each field of view was imaged for 60 seconds, and each second a stack
671 of 6 z-slices separated by 0.5 μm was imaged. The microscope was focused such
672 that the part of the cell closest to the coverslip was captured.
673

674 **Acute hypotonic shocks**

675 Walled cells or protoplasts were first imaged in their steady state media
676 (EMM5S supplemented with 0 to 1.2 M D-Sorbitol). The steady state media was
677 exchanged with media supplemented with a lower D-Sorbitol concentration (the
678 concentration difference is noted ΔC), with inlet pressure of 5 psi. This hypotonic
679 shock media was labelled with 6.7 $\mu\text{g/mL}$ of sulforhodamine B (MP Biomedicals LLC,
680 Santa Ana, USA), a red cell-impermeable dye that allowed us to a) monitor the full
681 exchange of the solution in the microfluidic chamber prior to image acquisition, and
682 b) monitor the plasma membrane integrity of the cells after the shock. In each
683 condition, the first movie was started when the sulforhodamine B dye was visible in

684 the field of view. For clarity, this time point is labelled $t=0$ min in all our figures, but
685 note that we estimate it may vary by up to ~30 seconds between movies and
686 conditions. We imaged cells by taking one stack of 6 Z-slices per second for 60
687 seconds. After the end of each movie, we rapidly changed field of view and restarted
688 acquisition one minute after the end of the previous movie, so that movies started
689 every 2 minutes after the acute hypotonic shock. Tracks from cells that contained red
690 fluorescence from the sulforhodamine B dye were excluded from the analysis,
691 because this indicated that cell membrane had been damaged.

692

693 **Inhibition of endocytosis and exocytosis during acute hypotonic shock**

694 Endocytosis or exocytosis was inhibited by including respectively 25 μ M
695 Latrunculin A (Millipore, MA, USA) or 2mM Brefeldin A (Santa Cruz Biotechnology
696 Inc., TX, USA) in the solution used to prepare the protoplasts and and to perform the
697 hypotonic shocks. Hypotonic shock solution also included 20 μ M FM4-64 (Biotium,
698 Fremont, CA, USA) to stain dead protoplasts (Vida and Gerhardt, 1999) (Figure 5A),
699 and inlet pressure was set at 4 psi.

700

701 **Measurement of the temporal evolution of the number of proteins and speed**

702 Movies were processed and analyzed using an updated version of the
703 PatchTrackingTools toolset for the Fiji (Schindelin et al., 2012) distribution of ImageJ
704 (Berro and Pollard, 2014a; Schneider et al., 2012). This new version includes
705 automatic patch tracking capabilities based on the Trackmate library (Tinevez et al.,
706 2017), and is available on the Berro lab website:
707 [http://campuspress.yale.edu/berrolab/
708 publications/software/](http://campuspress.yale.edu/berrolab/publications/software/). Prior to any quantitative measurements, we corrected our
709 movies for uneven illumination and camera noise. The uneven illumination was
710 measured by imaging a solution of Alexa 488 dye and the camera noise was
711 measured by imaging a field of view with 0% laser power. We tracked Fim1-mEGFP
712 spots with a circular 7-pixel diameter region of interest (ROI), and measured the
713 temporal evolution of the fluorescence intensities and the position of the centers of
714 mass. The spot intensity was corrected for cytoplasmic background using a 9-pixel
715 median filter, and was then corrected for photobleaching. The photobleaching rate
716 was estimated by fitting a single exponential to the temporal evolution of the intensity
717 of cytoplasmic ROIs void of any identifiable spots of fluorescence (Berro and Pollard,
718 2014a). Only tracks longer than 5 s and displaying an increase followed by a
719 decrease in intensity were kept for the analysis. Individual tracks were aligned and
720 averaged with the temporal super-resolution algorithm from (Berro and Pollard,
721 2014a), and post-processed using custom scripts in Matlab R2016a (Mathworks). In
722 brief, this method realigns temporal signals that have low temporal resolution and
723 where no absolute time reference is available to align them relatively to each other. It
724 iteratively finds the temporal offset which has a higher precision than the measured
725 signal and minimizes the mean square difference between each measured signal
726 and a reference signal. For the first round of alignments, the reference signal is one
727 of the measurements. After each realignment round, a new reference is calculated as
728 the mean of all the realigned signals, which is an estimator of the true underlying
729 signal.

730 To control and calibrate the intensity of our measurements, we imaged wild-
731 type walled cell expressing Fim1p-mEGP each imaging day. Intensities were
732 converted into number of molecules with a calibration factor such that the peak
733 intensity of our control strain corresponded to 830 molecules (Berro and Pollard,

734 2014a).

735 In all figures presenting the temporal evolution of the number of molecules or
736 the speed, time 0 s corresponds to the time point when the number of molecules is
737 maximum (also called the peak number). The “speed vs time” plots helps determine
738 whether endocytosis completes normally in different conditions. At a given time point,
739 the speed corresponds to the average movement of the endocytic structure in the
740 plane of the membrane between two consecutive images. For an endocytic event
741 that completes normally, the speed is close to 0 while the endocytic pit elongates
742 before the vesicle is pinched off. Note that the speed is not exactly 0 because of
743 localization errors and putative small movements of the endocytic structure in the
744 plane of the membrane. The speed increases after the vesicle is pinched off and it
745 diffuses freely in the cytoplasm. Since this movement is mostly diffusive, the standard
746 deviations of the speeds are large.

747 Statistical tests between conditions were performed at time 0 s with a one-way
748 ANOVA test using the number of tracks collected to build the figure. To avoid
749 extrapolating the data, we compared the relative duration of assembly and
750 disassembly between conditions using the time at which the average number of
751 molecules reach half the peak number.

752

753 **Measurement of the density of CME events**

754 We used the *S. Pombe* profiling tools for ImageJ (Berro and Pollard, 2014a) to
755 measure the number of endocytic events at a given time in each cell. In brief, on a
756 sum-projected z-stack, we manually outlined individual cells, and, for each position
757 along the long axis of a cell, we measured the sum of fluorescence orthogonal to the
758 long axis. We corrected the intensity profile in each cell for its cytoplasmic intensity
759 and media fluorescence outside the cell. We estimated the number of patches in
760 each cell by dividing the corrected fluorescence signal with the temporal average of
761 the fluorescence intensity of one endocytic event. We calculated the linear density of
762 endocytic events as the ratio between the number of endocytic events in a cell and
763 its length.

764 We estimated the percentage of plasma membrane internalized by
765 endocytosis per minute as follows. We measured ~120 endocytic sites per cell at a
766 given time on average. Since the actin meshwork assembles and disassembles in
767 about 20 seconds, we estimate that 360 endocytic vesicles are formed per minute.
768 Assuming endocytic vesicles have a 50-nm diameter, this corresponds to a ~2.8 μm^2
769 endocytosed per minute, or ~2% of the total surface area, considering the average
770 cell is around 12 μm long and has a 132 μm^2 of plasma membrane (assuming the
771 cell shape is a cylinder capped by two hemispheres).

772 **Measurement of the exocytosis rate with FM4-64 staining**

773 The exocytosis rate was measured by combining the acute hypotonic shock
774 with FM4-64 staining, in a similar approach as has been reported (Gauthier et al.,
775 2009; Smith and Betz, 1996; Vida and Emr, 1995). The cell impermeable dye FM4-
776 64 (Biotium, Fremont, CA, USA) was diluted to a final concentration of 20 μM in any
777 of the media used. When cells are exposed to FM4-64, the dye rapidly stains the
778 outer leaflet of the plasma membrane. Upon endocytosis, the dye is trafficked inside
779 the cell without change in fluorescence. The total cell fluorescence intensity was
780 measured after segmenting the cells by thresholding the fluorescence signal above
781 background levels. The fluorescence intensity was normalized to the intensity
782 reached at the end of the fast increase ~1 min after the dye was flowed in, which

783 corresponds to the intensity of total surface area of the plasma membrane (Figure
784 4B). After this fast phase (< 20 seconds), the fluorescence signal increased more
785 slowly every time unstained membrane was exposed to the cell surface by
786 exocytosis. At short time scale (~5 to 20 min depending on the exocytosis rate),
787 recycling of stained membrane is negligible and one can assume that all exocytosed
788 membrane is virtually unstained. Since the intensity at the beginning of the slow
789 phase was normalized to 1, the slope of the linear increase of fluorescence is equal
790 to the amount of membrane exocytosed per minute, expressed as a fraction of the
791 surface area of the plasma membrane. For all measurements, images were taken at
792 5 s interval at the middle plane of cells with the help of Perfect Focusing System
793 (Nikon, Tokyo, Japan), with minimal laser excitation in order to reduce toxicity and
794 photobleaching to negligible values. Curve fitting and slope calculation was
795 performed in GraphPad Prism (GraphPad Software, La Jolla, CA, USA).

796 797 **Measurement of eisosomes' density on the plasma membrane**

798 We imaged full cells expressing Pil1p-mEGFP by taking stacks of 0.5 μm
799 spaced Z-slices. We corrected these Z-stacks for uneven illumination and manually
800 outlined individual cells to determine the surface area of each cell. To determine the
801 total amount of eisosome-bound Pil1p-mEGFP we subtracted the cytosolic intensity
802 of Pil1-mEGFP using a pre-determined threshold and summed all the Z-slices. We
803 measured the mean membrane intensity of each cell on the thresholded sum-
804 projection image. The eisosome density was determined by dividing this mean
805 intensity by the surface area of each protoplast.

806 To quantify the relative changes in area fraction of eisosomes after acute
807 hypotonic shock, wild-type protoplasts expressing Pil1p-mEGFP were loaded into
808 ONIX2 microfluidics system (Millipore-Sigma, Saint-Louis, USA), and time-lapse
809 fluorescent images were taken at a single Z-slice at the top of protoplasts during
810 media change. After background correction, the total area fraction of eisosomes at
811 the beginning of hypotonic shock was set to 1.0 for normalization, and the normalized
812 values of area fraction were fit to a single exponential decay curve in GraphPad
813 Prism (GraphPad Software, La Jolla, CA, USA).

814

815 **Measurement of membrane tension**

816 Protoplasts were loaded in a custom-built chamber which was passivated with
817 0.2 mg/mL β -casein (Millipore-Sigma, Saint-Louis, USA) for 30 minutes and pre-
818 equilibrated with EMM5S supplemented with 0.8 M D-Sorbitol. A glass micropipette
819 (#1B100-4, World Precision Instruments, Sarasota, USA) was forged to a diameter
820 smaller than the average protoplast radius (~2.5 μm), and was connected to a water
821 reservoir of adjustable height to apply a defined aspiration pressure. Before and after
822 each experiment the height of the water reservoir was adjusted to set the aspiration
823 pressure to 0. Cells were imaged with a bright field IX-71 inverted microscope
824 (Olympus, Tokyo, Japan) equipped with a 60X/1.4NA objective, and images were
825 recorded every second. Aspiration pressure was gradually increased every 30 s and
826 the membrane tension σ was calculated as $\sigma = \Delta P \cdot R_p / [2(1 - R_p/R_c)]$, where R_p and
827 R_c are respectively the micropipette and the cell radius, ΔP is the aspiration pressure
828 for which the length of the tongue l of the protoplast in the micropipette is equal to R_p
829 (Evans and Yeung, 1989). To limit the effects of the adaptation of cells' membrane
830 tension, all measurements were performed within the first five minutes after the
831 hypotonic shock, which greatly limited the throughput of our assay (1 measurement

832 per sample), compared to the measurements at steady state (around 6
833 measurements per sample).

834

835

836 **Acknowledgements**

837 We thank Yale West Campus Imaging core for providing access to the spinning disc
838 confocal microscope, members of the Berro lab for insightful discussions and R.
839 Fernandez for providing mutant yeast strains. We thank Ramesh Ramji and Kathryn
840 Miller-Jensen for initial help with the microfluidics part of this project. We gratefully
841 thank Millipore Sigma for lending us a CellASIC unit and Erdem Karatekin for access
842 to his micropipette aspiration setup. We also thank Samantha Dundon, Mike Lacy
843 and Matt Akamatsu for their comments on our manuscript. This research was
844 supported in part by National Institutes of Health/National Institute of General Medical
845 Sciences Grant R01GM115636 and by seed funding from the American Cancer
846 Society Institutional Research Grant #IRG 58-012-58.

847

References

- 849 Aghamohammadzadeh S, Ayscough KR. 2009. Differential requirements for actin during
850 yeast and mammalian endocytosis. *Nature cell biology* **11**:1039–1042.
851 doi:10.1038/ncb1918
- 852 Aghamohammadzadeh S, Smaczynska-de Rooij II, Ayscough KR. 2014. An Abp1-dependent
853 route of endocytosis functions when the classical endocytic pathway in yeast is
854 inhibited. *PLoS ONE* **9**. doi:10.1371/journal.pone.0103311
- 855 Apodaca G. 2002. Modulation of membrane traffic by mechanical stimuli. *American Journal*
856 *of Physiology-Renal Physiology* **282**:F179–F190.
857 doi:10.1152/ajprenal.2002.282.2.F179
- 858 Arasada R, Pollard TD. 2011. Distinct Roles for F-BAR Proteins Cdc15p and Bzz1p in Actin
859 Polymerization at Sites of Endocytosis in Fission Yeast. *Current Biology* **21**:1450–
860 1459. doi:10.1016/j.cub.2011.07.046
- 861 Arasada R, Sayyad WAWA, Berro J, Pollard TDTD. 2018. High-speed superresolution
862 imaging of the proteins in fission yeast clathrin-mediated endocytic actin patches.
863 *Molecular Biology of the Cell* **29**:295–303. doi:10.1091/mbc.E17-06-0415
- 864 Atilgan E, Magidson V, Khodjakov A, Chang F. 2015. Morphogenesis of the Fission Yeast
865 Cell through Cell Wall Expansion. *Current biology* □: *CB* **25**:2150–7.
866 doi:10.1016/j.cub.2015.06.059
- 867 Basu R, Munteanu EL, Chang F. 2013. Role of turgor pressure in endocytosis in fission yeast.
868 *Molecular biology of the cell* **25**:679–87. doi:10.1091/mbc.E13-10-0618
- 869 Berro J, Lacy MM. 2018. Quantitative Biology of Endocytosis, Colloquium Series on
870 Quantitative Cell Biology (Marshall WF, ed). San Rafael (CA): Morgan & Claypool.
- 871 Berro J, Pollard TD. 2014a. Local and global analysis of endocytic patch dynamics in fission
872 yeast using a new “temporal superresolution” realignment method. *MBoC* **25**:3501–
873 3514. doi:10.1091/mbc.E13-01-0004
- 874 Berro J, Pollard TD. 2014b. Synergies between Aip1p and capping protein subunits (Acp1p
875 and Acp2p) in clathrin-mediated endocytosis and cell polarization in fission yeast.
876 *MBoC* **25**:3515–3527. doi:10.1091/mbc.E13-01-0005
- 877 Berro J, Sirotkin V, Pollard TD. 2010. Mathematical modeling of endocytic actin patch
878 kinetics in fission yeast: disassembly requires release of actin filament fragments.
879 *MBoC* **21**:2905–2915. doi:10.1091/mbc.E10-06-0494
- 880 Boulant S, Kural C, Zeeh J-C, Ubelmann F, Kirchhausen T. 2011. Actin dynamics counteract
881 membrane tension during clathrin-mediated endocytosis. *Nature cell biology* **13**:1124–
882 1131. doi:10.1038/ncb2307
- 883 Burke TA, Christensen JR, Barone E, Suarez C, Sirotkin V, Kovar DR. 2014. Homeostatic
884 actin cytoskeleton networks are regulated by assembly factor competition for
885 monomers. *Current Biology* **24**:579–585. doi:10.1016/j.cub.2014.01.072
- 886 Carlsson AE, Bayly P V. 2014. Force generation by endocytic actin patches in budding yeast.
887 *Biophysical Journal* **106**:1596–1606. doi:10.1016/j.bpj.2014.02.035
- 888 Chen Q, Pollard TD. 2013. Actin Filament Severing by Cofilin Dismantles Actin Patches and
889 Produces Mother Filaments for New Patches. *Current Biology* **23**:1154–1162.
890 doi:10.1016/J.CUB.2013.05.005
- 891 Cheng JPX, Mendoza-Topaz C, Howard G, Chadwick J, Shvets E, Cowburn AS, Dunmore
892 BJ, Crosby A, Morrell NW, Nichols BJ. 2015. Caveolae protect endothelial cells from
893 membrane rupture during increased cardiac output. *The Journal of Cell Biology*
894 **211**:53–61. doi:10.1083/jcb.201504042

- 895 Cochilla AJ, Angleson JK, Betz WJ. 1999. MONITORING SECRETORY MEMBRANE
896 WITH FM1-43 FLUORESCENCE. *Annual Review of Neuroscience* **22**:1–10.
897 doi:10.1146/annurev.neuro.22.1.1
- 898 Courtemanche N, Pollard TD, Chen Q. 2016. Avoiding artefacts when counting polymerized
899 actin in live cells with LifeAct fused to fluorescent proteins. *Nature Cell Biology*
900 **18**:676–683. doi:10.1038/ncb3351
- 901 Davì V, Tanimoto H, Ershov D, Haupt A, De Belly H, Le Borgne R, Couturier E, Boudaoud
902 A, Minc N. 2018. Mechanosensation Dynamically Coordinates Polar Growth and Cell
903 Wall Assembly to Promote Cell Survival. *Developmental cell* **45**:170-182.e7.
904 doi:10.1016/j.devcel.2018.03.022
- 905 Dmitrieff S, Nédélec F. 2015. Membrane Mechanics of Endocytosis in Cells with Turgor.
906 *PLoS Computational Biology* **11**. doi:10.1371/journal.pcbi.1004538
- 907 Evans E, Yeung a. 1989. Apparent viscosity and cortical tension of blood granulocytes
908 determined by micropipet aspiration. *Biophysical journal* **56**:151–160.
909 doi:10.1016/S0006-3495(89)82660-8
- 910 Ferguson JP, Huber SD, Willy NM, Aygün E, Goker S, Atabey T, Kural C. 2017.
911 Mechanoregulation of clathrin-mediated endocytosis. *Journal of Cell Science*
912 **130**:3631–3636. doi:10.1242/jcs.205930
- 913 Ferguson S, Raimondi A, Paradise S, Shen H, Mesaki K, Ferguson A, Destaing O, Ko G,
914 Takasaki J, Cremona O, O' Toole E, De Camilli P. 2009. Coordinated Actions of
915 Actin and BAR Proteins Upstream of Dynamin at Endocytic Clathrin-Coated Pits.
916 *Developmental Cell* **17**:811–822. doi:10.1016/j.devcel.2009.11.005
- 917 Flor-Parra I, Zhurinsky J, Bernal M, Gallardo P, Daga RR. 2014. A Lallzyme MMX-based
918 rapid method for fission yeast protoplast preparation. *Yeast* **31**:61–66.
919 doi:10.1002/yea.2994
- 920 Gachet Y, Hyams JS. 2005. Endocytosis in fission yeast is spatially associated with the actin
921 cytoskeleton during polarised cell growth and cytokinesis. *Journal of Cell Science*
922 **118**:4231–4242. doi:10.1242/jcs.02530
- 923 Gauthier NC, Rossier OM, Mathur A, Hone JC, Sheetz MP. 2009. Plasma Membrane Area
924 Increases with Spread Area by Exocytosis of a GPI-anchored Protein Compartment.
925 *Molecular Biology of the Cell* **20**:3261–3272. doi:10.1091/mbc.e09-01-0071
- 926 Goode BL, Eskin JA, Wendland B. 2015. Actin and endocytosis in budding yeast. *Genetics*
927 **199**:315–58. doi:10.1534/genetics.112.145540
- 928 Hassinger JE, Oster G, Drubin DG, Rangamani P. 2017. Design principles for robust
929 vesiculation in clathrin-mediated endocytosis. *Proceedings of the National Academy*
930 *of Sciences* **114**:E1118–E1127. doi:10.1073/pnas.1617705114
- 931 Homann U. 1998. Fusion and fission of plasma-membrane material accommodates for
932 osmotically induced changes in the surface area of guard-cell protoplasts. *Planta*
933 **206**:329–333. doi:10.1007/s004250050408
- 934 Kabeche R, Howard L, Moseley JB. 2015. Eisosomes provide membrane reservoirs for rapid
935 expansion of the yeast plasma membrane. *Journal of Cell Science* **128**:4057–4062.
936 doi:10.1242/jcs.176867
- 937 Lacy MM, Baddeley D, Berro J. 2019. Single-molecule turnover dynamics of actin and
938 membrane coat proteins in clathrin-mediated endocytosis. *eLife* **8**:e52355.
939 doi:10.7554/elife.52355
- 940 Lacy MM, Baddeley D, Berro J. 2017. Single-molecule imaging of the BAR-domain protein
941 Pil1p reveals filament-end dynamics. *MBoC* **28**:2251–2259. doi:10.1091/mbc.e17-04-
942 0238

- 943 Lacy MM, Ma R, Ravindra NG, Berro J. 2018. Molecular mechanisms of force production in
944 clathrin-mediated endocytosis. *FEBS Letters* **592**:3586–3605. doi:10.1002/1873-
945 3468.13192
- 946 Lo HP, Hall TE, Parton RG. 2016. Mechanoprotection by skeletal muscle caveolae.
947 *BioArchitecture* **0992**:00–00. doi:10.1080/19490992.2015.1131891
- 948 Lo Presti L, Chang F, Martin SG. 2012. Myosin Vs organize actin cables in fission yeast.
949 *Molecular Biology of the Cell*. doi:10.1091/mbc.E12-07-0499
- 950 Ma R, Berro J. 2021. Endocytosis against high turgor pressure is made easier by partial
951 protein coating and a freely rotating base. *Biophysical Journal*.
952 doi:10.1016/j.bpj.2021.02.033
- 953 Ma R, Berro J. 2019. Crosslinking actin networks produces compressive force. *Cytoskeleton*
954 **76**:346–354. doi:10.1002/cm.21552
- 955 Ma R, Berro J. 2018. Structural organization and energy storage in crosslinked actin
956 assemblies. *PLOS Computational Biology* **14**:e1006150.
957 doi:10.1371/journal.pcbi.1006150
- 958 Minc N, Boudaoud A, Chang F. 2009. Mechanical forces of fission yeast growth. *Current*
959 *biology*: *CB* **19**:1096–1101. doi:10.1016/j.cub.2009.05.031
- 960 Morris CE, Homann U. 2001. Cell Surface Area Regulation and Membrane Tension. *The*
961 *Journal of Membrane Biology* **179**:79–102. doi:10.1007/s002320010040
- 962 Moseley JB. 2018. Eisosomes. *Current Biology* **28**:R376–R378.
963 doi:10.1016/J.CUB.2017.11.073
- 964 Mostov KE, Verges M, Altschuler Y. 2000. Membrane traffic in polarized epithelial cells.
965 *Current Opinion in Cell Biology* **12**:483–490. doi:10.1016/S0955-0674(00)00120-4
- 966 Nicholson-Fish JC, Smillie KJ, Cousin MA. 2016. Monitoring activity-dependent bulk
967 endocytosis with the genetically-encoded reporter VAMP4-pHluorin. *Journal of*
968 *Neuroscience Methods* **266**:1–10. doi:10.1016/j.jneumeth.2016.03.011
- 969 Palmer SE, Smaczynska-de Rooij II, Marklew CJ, Allwood EG, Mishra R, Johnson S,
970 Goldberg MW, Ayscough KR. 2015. A dynamin-actin interaction is required for
971 vesicle scission during endocytosis in yeast. *Current Biology* **25**:868–878.
972 doi:10.1016/j.cub.2015.01.061
- 973 Parton RG, Pozo MA del, Vassilopoulos S, Nabi IR, Lay SL, Lundmark R, Kenworthy AK,
974 Camus A, Blouin CM, Sessa WC, Lamaze C. 2019. Caveolae: The FAQs. *Traffic n/a*.
975 doi:10.1111/tra.12689
- 976 Picco A, Kukulski W, Manenschijn HE, Specht T, Briggs JAG, Kaksonen M, Lemmon S.
977 2018. The contributions of the actin machinery to endocytic membrane bending and
978 vesicle formation. *MBoC* **29**:1346–1358. doi:10.1091/mbc.E17-11-0688
- 979 Planade J, Belbahri R, Sanders MB, Guillotin A, Roure O du, Michelot A, Heuvingsh J. 2019.
980 Mechanical stiffness of reconstituted actin patches correlates tightly with endocytosis
981 efficiency. *PLOS Biology* **17**:e3000500. doi:10.1371/journal.pbio.3000500
- 982 Reinisch KM, Prinz WA. 2021. Mechanisms of nonvesicular lipid transport. *Journal of Cell*
983 *Biology* **220**. doi:10.1083/jcb.202012058
- 984 Richards DA, Guatimosim C, Betz WJ. 2000. Two Endocytic Recycling Routes Selectively
985 Fill Two Vesicle Pools in Frog Motor Nerve Terminals. *Neuron* **27**:551–559.
986 doi:10.1016/S0896-6273(00)00065-9
- 987 Riggi M, Bourgoing C, Macchione M, Matile S, Loewith R, Roux A. 2019. TORC2 controls
988 endocytosis through plasma membrane tension. *The Journal of Cell Biology*.
989 doi:10.1083/jcb.201901096
- 990 Riggi M, Niewola-Staszewska K, Chiaruttini N, Colom A, Kusmider B, Mercier V,
991 Soleimanpour S, Stahl M, Matile S, Roux A, Loewith R. 2018. Decrease in plasma

- 992 membrane tension triggers PtdIns(4,5)P₂ phase separation to inactivate TORC2.
993 *Nature Cell Biology* **20**:1043–1051. doi:10.1038/s41556-018-0150-z
- 994 Schaber J, Adrover MÀ, Eriksson E, Pelet S, Petelenz-Kurdziel E, Klein D, Posas F, Goksör
995 M, Peter M, Hohmann S, Klipp E. 2010. Biophysical properties of *Saccharomyces*
996 *cerevisiae* and their relationship with HOG pathway activation. *European Biophysics*
997 *Journal* **39**:1547–1556. doi:10.1007/s00249-010-0612-0
- 998 Schindelin J, Arganda-Carreras I, Frise E, Kaynig V, Longair M, Pietzsch T, Preibisch S,
999 Rueden C, Saalfeld S, Schmid B, Tinevez JY, White DJ, Hartenstein V, Eliceiri K,
1000 Tomancak P, Cardona A. 2012. Fiji: An open-source platform for biological-image
1001 analysis. *Nature Methods*. doi:10.1038/nmeth.2019
- 1002 Schneider CA, Rasband WS, Eliceiri KW. 2012. NIH Image to ImageJ: 25 years of image
1003 analysis. *Nature Methods* **9**:671–675. doi:10.1038/nmeth.2089
- 1004 Sens P, Turner MS. 2006. Budded membrane microdomains as tension regulators. *Physical*
1005 *Review E - Statistical, Nonlinear, and Soft Matter Physics* **73**:1–4.
1006 doi:10.1103/PhysRevE.73.031918
- 1007 Sinha B, Köster D, Ruez R, Gonnord P, Bastiani M, Abankwa D, Stan R V., Butler-Browne
1008 G, Védie B, Johannes L, Morone N, Parton RG, Raposo G, Sens P, Lamaze C, Nassoy
1009 P. 2011. Cells respond to mechanical stress by rapid disassembly of caveolae. *Cell*
1010 **144**:402–413. doi:10.1016/j.cell.2010.12.031
- 1011 Sirotkin V, Berro J, Macmillan K, Zhao L, Pollard TD. 2010. Quantitative analysis of the
1012 mechanism of endocytic actin patch assembly and disassembly in fission yeast.
1013 *Molecular biology of the cell* **21**:2894–904. doi:10.1091/mbc.E10-02-0157
- 1014 Skau CT, Courson DS, Bestul AJ, Winkelman JD, Rock RS, Sirotkin V, Kovar DR. 2011.
1015 Actin filament bundling by fimbrin is important for endocytosis, cytokinesis, and
1016 polarization in fission yeast. *The Journal of biological chemistry* **286**:26964–77.
1017 doi:10.1074/jbc.M111.239004
- 1018 Smith CB, Betz WJ. 1996. Simultaneous independent measurement of endocytosis and
1019 exocytosis. *Nature* **380**:531–534. doi:10.1038/380531a0
- 1020 Stachowiak MR, Laplante C, Chin HF, Guirao B, Karatekin E, Pollard TD, O’Shaughnessy B.
1021 2014. Mechanism of cytokinetic contractile ring constriction in fission yeast.
1022 *Developmental cell* **29**:547–61. doi:10.1016/j.devcel.2014.04.021
- 1023 Suarez C, Carroll RT, Burke TA, Christensen JR, Bestul AJ, Sees JA, James ML, Sirotkin V,
1024 Kovar DR. 2015. Profilin Regulates F-Actin Network Homeostasis by Favoring
1025 Formin over Arp2/3 Complex. *Developmental Cell* **32**:43–53.
1026 doi:10.1016/J.DEVCEL.2014.10.027
- 1027 Tinevez JY, Perry N, Schindelin J, Hoopes GM, Reynolds GD, Laplantine E, Bednarek SY,
1028 Shorte SL, Eliceiri KW. 2017. TrackMate: An open and extensible platform for
1029 single-particle tracking. *Methods* **115**:80–90. doi:10.1016/j.ymeth.2016.09.016
- 1030 Urbina FL, Gomez SM, Gupton SL. 2018. Spatiotemporal organization of exocytosis emerges
1031 during neuronal shape change. *Journal of Cell Biology* **217**:1113–1128.
1032 doi:10.1083/jcb.201709064
- 1033 Vida T, Gerhardt B. 1999. A Cell-Free Assay Allows Reconstitution of Vps33p-Dependent
1034 Transport to the Yeast Vacuole/Lysosome. *J Cell Biol* **146**:85–98.
- 1035 Vida TA, Emr SD. 1995. A new vital stain for visualizing vacuolar membrane dynamics and
1036 endocytosis in yeast. *The Journal of cell biology* **128**:779–92.
1037 doi:10.1083/JCB.128.5.779
- 1038 Walther TC, Aguilar PS, Fröhlich F, Chu F, Moreira K, Burlingame AL, Walter P. 2007. Pkh-
1039 kinases control eisosome assembly and organization. *The EMBO journal* **26**:4946–55.
1040 doi:10.1038/sj.emboj.7601933

1041 Watanabe S, Boucrot E. 2017. Fast and ultrafast endocytosis. *Current Opinion in Cell Biology*
1042 **47:64–71**. doi:10.1016/j.ceb.2017.02.013
1043

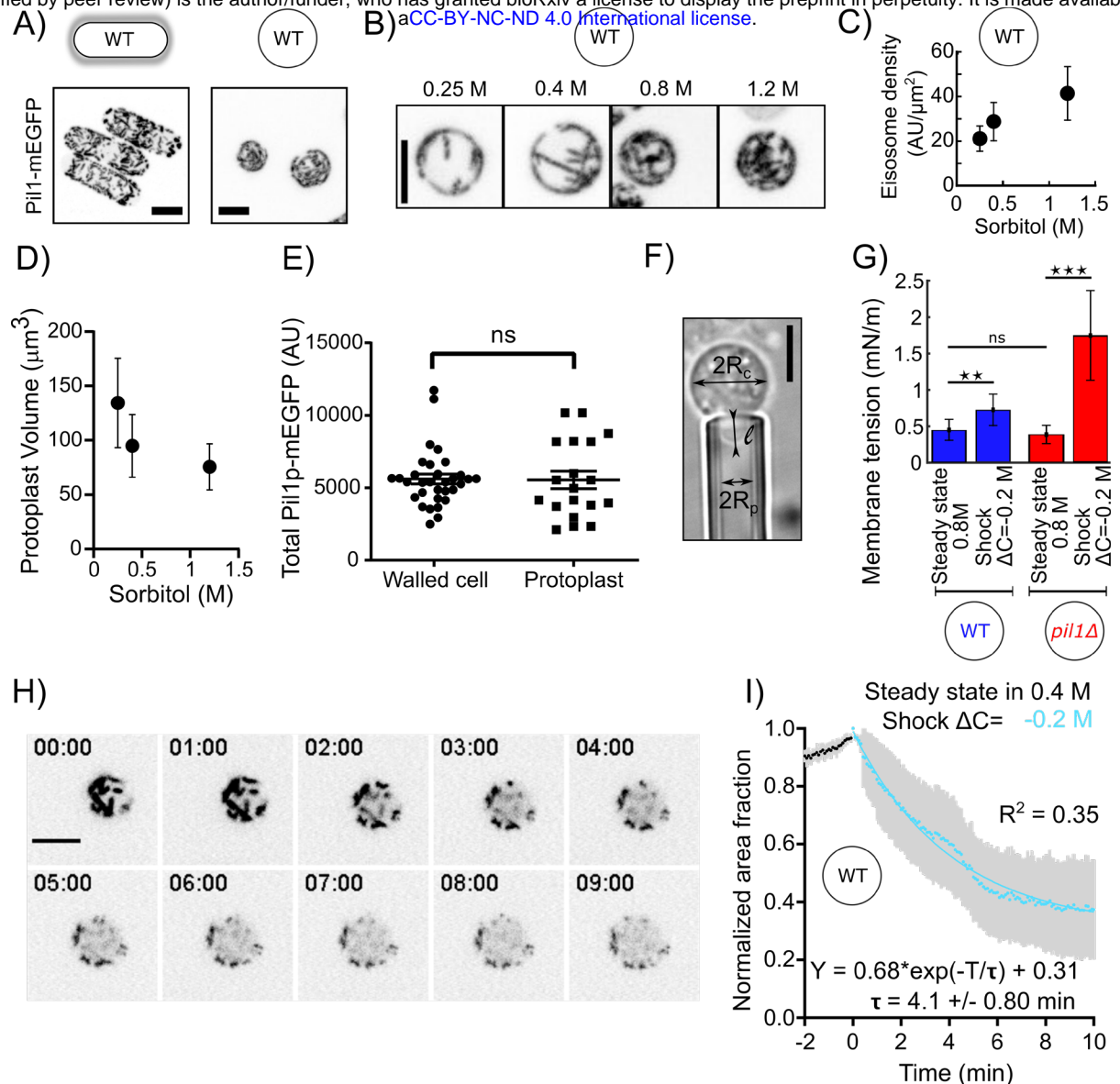


Figure 1: Eisosomes disassemble to buffer increases in membrane tension. A) Representative walled yeast cells (left column) and protoplasts (right column) at steady state in 1.2 M sorbitol expressing eisosome core protein Pil1-mEGFP (inverted contrast). Note that the cellular concentration of Pil1p-mEGFP is the same in walled cells and protoplasts (panel E). B) Eisosomes labelled with Pil1p-mEGFP (inverted contrast) in wild-type protoplasts at steady state in different sorbitol concentrations. From left to right: 0.25 M, 0.4 M, 0.8 M and 1.2 M sorbitol. C and D) Density of eisosomes at the plasma membrane (C), measured as the ratio between the intensity of Pil1p-mEGFP on the plasma membrane and the surface area of the protoplast and volume (D), at steady state in 0.25 M (N=26), 0.4 M (N=34) and 1.2 M (N=39) sorbitol. Error bars: standard deviations. E) The total amount of Pil1-mEGFP in walled cells (N=32) and protoplasts in 0.4 M sorbitol (N=19) are not significantly different (Mann-Whitney test, $P=0.65$). Each point represents one measurement, bars are the mean and SEM. F) Micropipette aspiration was used to measure membrane tension. R_c : cell radius; R_p : micropipette radius; l : length of the tongue inside the micropipette. G) Membrane tension of protoplasts at steady state in 0.8 M sorbitol and ~ 5 min after a hypotonic shock ($\Delta C = -0.2$ M) for wild-type (blue bars, N=28 for steady state and N=5

for the shock) and *pil1* Δ protoplasts (red bars, N=42 for steady state and N=7 for the shock). Error bars: standard deviation. p-values: non-significant (ns), $p>0.05$; two stars (**), $p\leq 0.01$; three stars (***), $p\leq 0.001$. H) and I) Eisosomes of wild-type protoplasts disassemble rapidly after a hypotonic shock. (H) Time course of a representative protoplast expressing Pil1p-mEGFP over 10 minutes after a hypotonic shock ($\Delta C = -0.2$ M) and initially at steady-state in 0.4 M sorbitol (just before time 0 min). (I) Evolution of the surface area covered by eisosomes over time, as a fraction of the surface area covered at time 0 min (normalized to 1). Data are from three independent experiments (N=15) and presented as mean \pm 95% confidence interval. Scale bars in (A), (B), (F) and (H): 5 μ m.

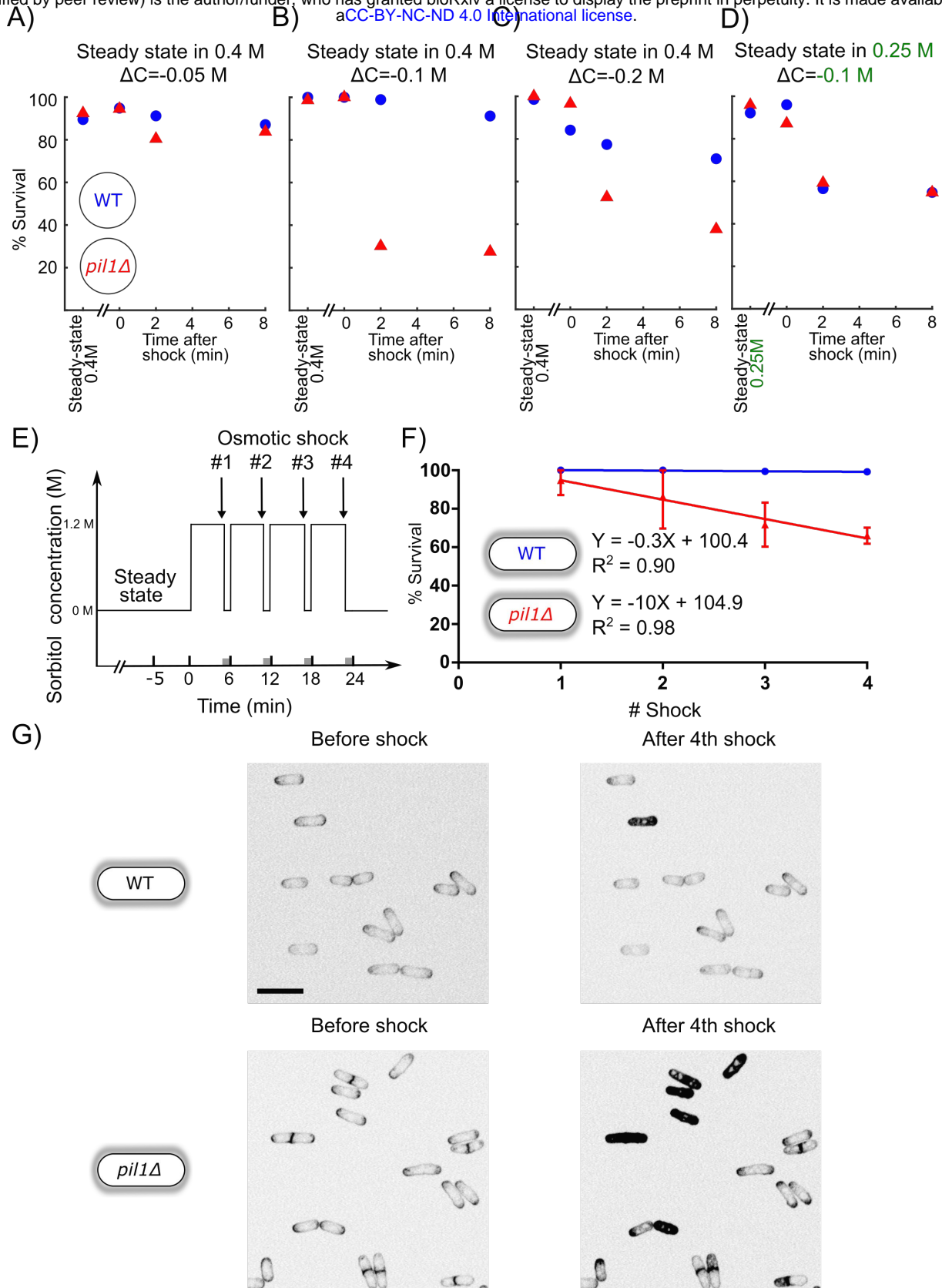


Figure 2: Eisosomes protect protoplasts and walled cells from osmotic shocks. A-C) Percentage of wild-type (blue dots) and *pil1* Δ (red triangle) protoplasts that are alive at steady-state in 0.4 M sorbitol, and after a $\Delta C = -0.05$ M (A), $\Delta C = -0.1$ M (B) and $\Delta C = -0.2$ M (C) single hypotonic shock. Representative fields of view used to

determine these percentages are shown in Figure 2 – Supplement 1. D) Percentage of wild-type (blue dots) and *pil1Δ* (red triangles) protoplasts that are alive at steady-state in 0.25 M sorbitol, and after a $\Delta C = -0.1$ M hypotonic shock. In these conditions, before the shock eisosomes in wild-type protoplasts are almost completely disassembled (Figure 1B). After the shock, wild-type cells survival is comparable to cells void of eisosomes because they lack Pil1p. E) Timeline of repeated $\Delta C = 1.2$ M osmotic shocks for walled cells. Each osmotic shock was performed by exchanging sorbitol concentration from 1.2 M (5 minutes) to 0 M (1 minute). F) Percentage of wild-type (blue dots, N=273) and *pil1Δ* (red triangle, N=197) walled cells that are alive after each osmotic shock. Note the progressive cell death induced by repeated osmotic shocks for *pil1Δ* cells. Combined data are from three independent experiments and plotted as mean \pm standard deviation. G) Representative images of wild-type (upper panel) and *pil1Δ* (lower panel) walled cells before shock and after the 4th shock. Dead cells are strongly stained by FM4-64 due to membrane damage. Scale bar: 10 μ m.

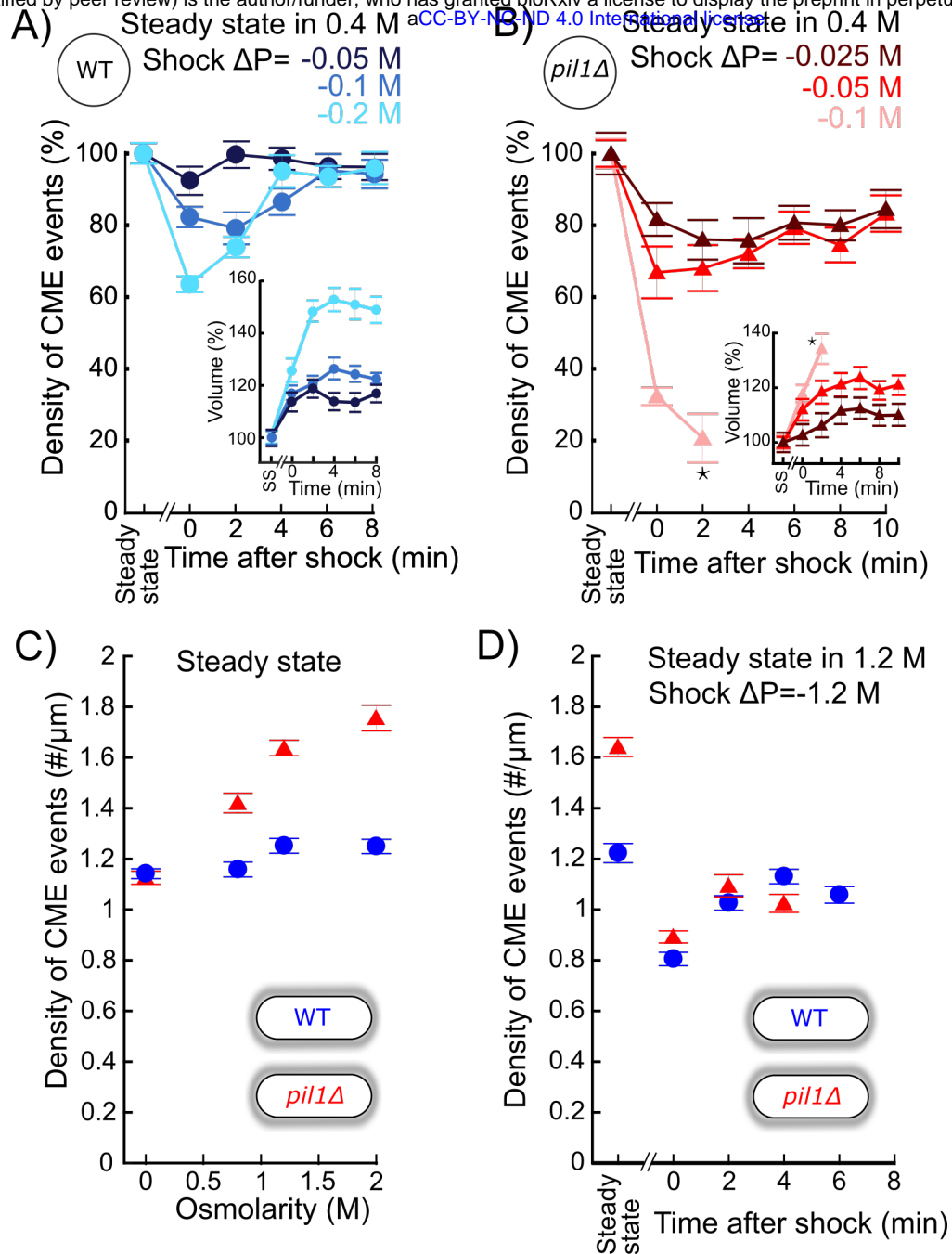


Figure 3: The density of endocytic events rapidly adapts after acute osmotic shocks.

A) Temporal evolution of density of endocytic events (average number of endocytic events at a given time in a cell divided by the cell length) in wild-type protoplasts initially at steady state in 0.4 M sorbitol and after an acute hypotonic shock of $\Delta C = -0.05$ M (dark blue, $N_{\text{cell}} \geq 102$), $\Delta C = -0.1$ M (blue, $N_{\text{cell}} \geq 54$) and $\Delta C = -0.2$ M (light blue, $N_{\text{cell}} \geq 83$). For $\Delta C = -0.1$ M and $\Delta C = -0.2$ M, the difference in the density of CME events between steady-state and 0 min or 2 min after the shock is statistically significant (one-way ANOVA, $p < 10^{-4}$). In all conditions, the difference after 6 min is not significant (one-way ANOVA, $p > 0.12$; details in the data file). B) Same as (A) but with *pil1Δ* protoplasts and hypotonic shocks of $\Delta C = -0.025$ M (dark red, $N_{\text{cell}} \geq 70$), $\Delta C = -0.05$ M (red, $N_{\text{cell}} \geq 103$) and $\Delta C = -0.1$ M (light red, $N_{\text{cell}} \geq 78$). In all conditions, the difference in the density of CME events between steady-state and any time after the shock is statistically significant (one-way ANOVA, $p < 10^{-3}$). For $\Delta C = -0.025$ M and

$\Delta C = -0.05$ M, the differences between time points after 6 min are not significant (one-way ANOVA, $p > 0.09$; details in the data file). (A) and (B) insets: relative volume increase after the hypotonic shocks (the volume at steady state is used as a reference). The numbers of cells used for each condition and each time point are given in Supplemental Table 2. The number of cells measured in the insets are the same as in the main figures. Star (*): the large majority of *pil1* Δ protoplasts were too damaged or dead 4 minutes after the hypotonic shocks at $\Delta C = -0.1$ M (Figure 2B), which prevented us to measure the density of endocytic events and the volume after this time point. C) Density of endocytic events in intact cells at steady state in different osmolarities, $N_{\text{cell}} \geq 80$. In *pil1* Δ walled cells, the difference in the density of CME events between all pairs of conditions is statistically significant (one-way ANOVA, $p < 10^{-4}$). In wild-type walled cells, the difference is small but statistically significant (details in the data file). The numbers of cells used for each condition and each time point are given in Supplemental Table 3. D) Density of endocytic events in wild-type (blue circle) and *pil1* Δ (red triangle) walled cells initially at steady state in 1.2 M sorbitol and after an acute hypotonic shock of $\Delta C = -1.2$ M, $N_{\text{cell}} \geq 44$. The numbers of cells used for each condition and each time point are given in Supplemental Table 4. For wild-type and *pil1* Δ walled cells, the differences in the density of CME events after 2 min are not statistically significant ($p > 0.08$; details in the data file). (A), (B), (C) and (D): error bars are standard errors of the mean.

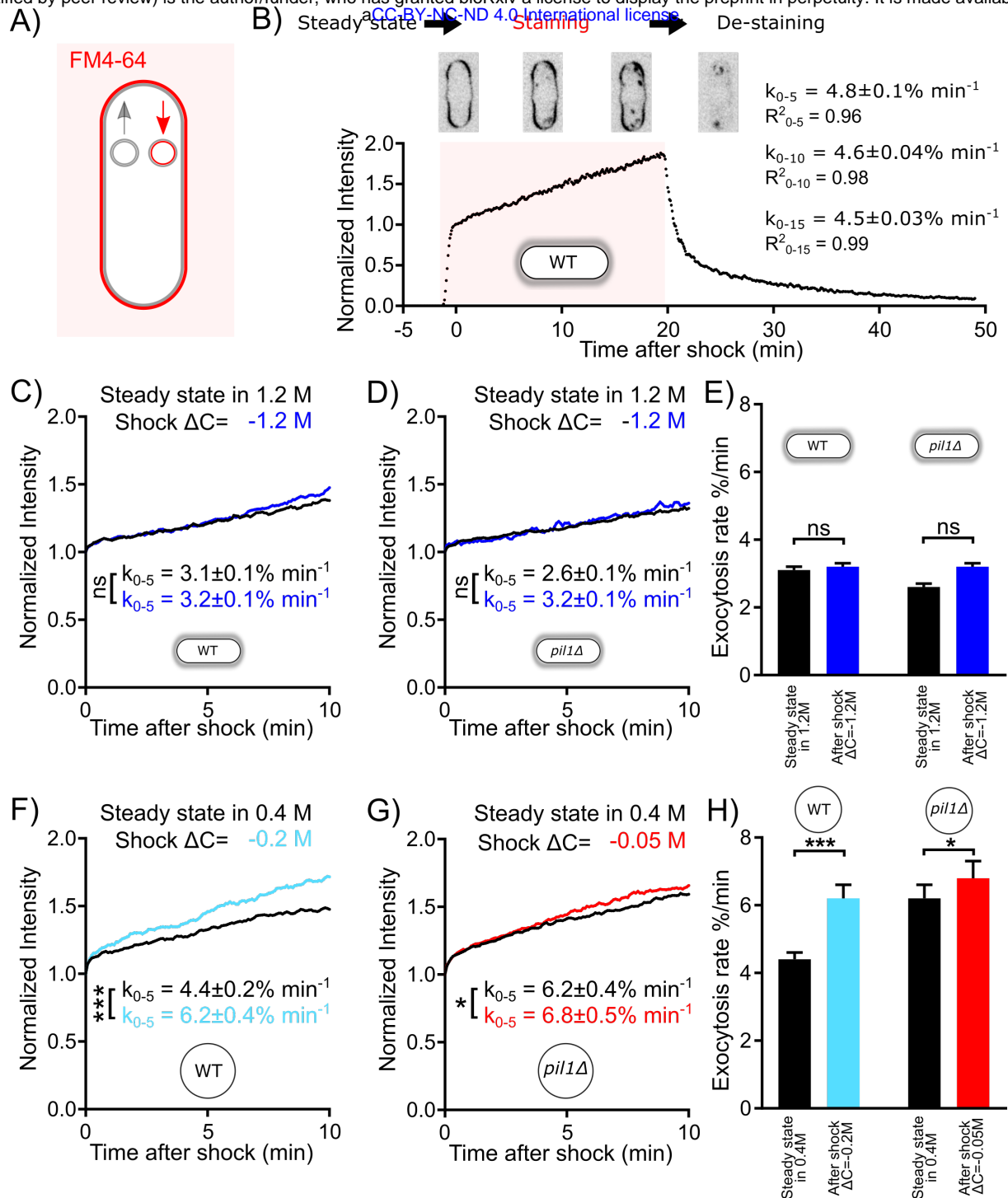


Figure 4: Exocytosis rate increases after an acute change in membrane tension in protoplasts but not in walled cells.

A) Rationale of measurement of whole cell exocytosis rate through FM4-64 staining. After FM4-64 is flown in the imaging chamber, the dye rapidly binds to the cell surface in less than a minute. After this initial phase, the whole cell fluorescence increases every time new (unlabeled) internal membrane is exposed to the cell surface by exocytosis. Note that endocytic events do not change the total fluorescence measured. **B)** Measurement of yeast cell exocytosis rate at steady state in 0 M sorbitol. Cells were stained with 20 μM FM4-64 in EMM5S for 20 min before washing with EMM5S. During FM4-64 staining, the fluorescence intensity increases rapidly for 1 min before entering a slow linear phase over at least 20 min for wild-type cells. The fluorescence intensity at the end of the

initial rapid increase phase corresponds to the complete staining of cell surface. It was normalized to 1, so that the subsequent increase in fluorescence intensity corresponds to a percentage of the plasma membrane surface area. After the dye was removed 20 min later, the decrease in fluorescence intensity suggests that the incorporation of FM4-64 didn't interfere with the vesicle trafficking pathway of the cell. The rate of exocytosis (measured as a percentage of the plasma membrane surface area per minute) is the slope of a linear fit of the measured signal over the first 5 min (k_{0-5}), 10 min (k_{0-10}) or 15 min (k_{0-15}). Example images of stained cells at different time points are shown in the middle panel (inverted contrast). (C) - (H) Rates of exocytosis at steady state and after hypotonic shocks. C) and D) The exocytic rate of wild-type walled cells is not changed after a $\Delta C = -1.2$ M acute hypotonic shock (black, before shock, $N_{\text{cells}} = 79$; blue, after shock, $N_{\text{cells}} = 68$; 3 replicates each). The exocytic rate of *pil1* Δ walled cells does not change significantly in the same conditions (black, before shock, $N_{\text{cells}} = 60$; blue, after shock, $N_{\text{cells}} = 96$; 3 replicates each). All walled cells were at steady-state in 1.2 M sorbitol before time 0 min. Curves for individual conditions in panels (C) and (D) are plotted in Figures 4 – Supplement 1A and 4 – Supplement 1B, respectively. E) Summary of exocytic rates for wild-type and *pil1* Δ walled cells before and after hypotonic shock. F) and G) The exocytic rate of wild-type and *pil1* Δ protoplasts increases after a $\Delta C = -0.2$ M (black, before shock, $N_{\text{cells}} = 20$; light blue, after shock, $N_{\text{cells}} = 37$; 4 replicates each) and $\Delta C = -0.05$ M (black, before shock, $N_{\text{cells}} = 44$; red, after shock, $N_{\text{cells}} = 60$; 4 replicates each) acute hypotonic shocks, respectively. Before time 0 min, all protoplasts were at steady-state in 0.4 M sorbitol. Curves for individual conditions in panels (F) and (G) are plotted in Figures 4 – Supplement 1C and 4 – Supplement 1D, respectively. H) Summary of exocytic rates for wild-type and *pil1* Δ protoplasts before and after hypotonic shock. (C) - (H) Data from at least three independent experiments were pooled together to produce each curve. p-values: non-significant (ns), $p > 0.05$; one star (*), $p \leq 0.05$; three stars (***), $p \leq 0.001$.

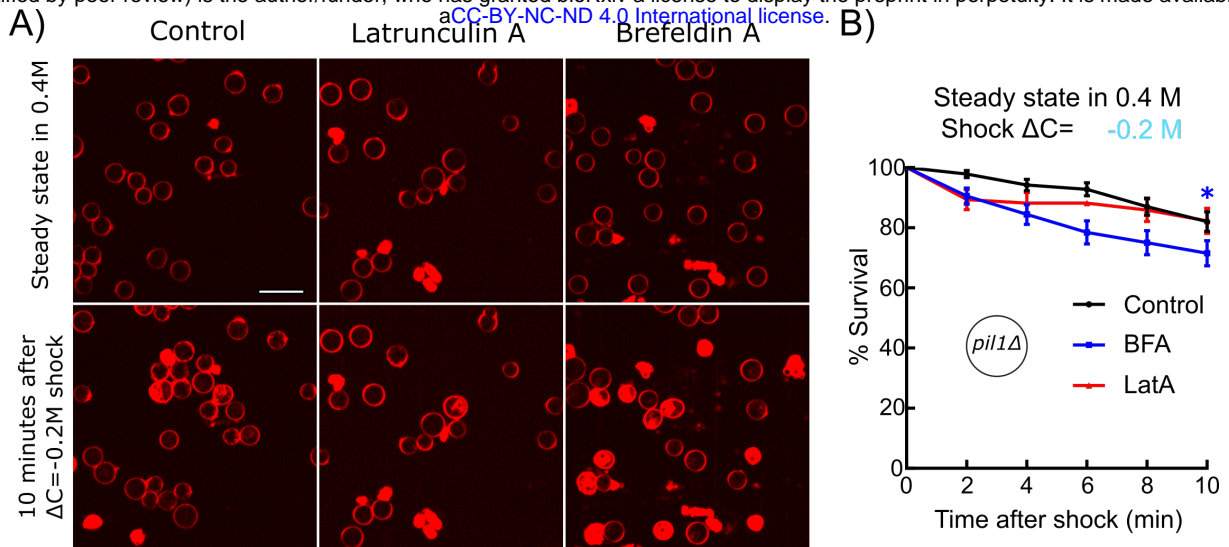


Figure 5: Inhibition of exocytosis but not endocytosis decreased the survival rate of protoplasts under acute hypotonic shock. A) *pil1Δ* protoplasts initially at steady state in 0.4 M sorbitol and supplemented with 25 μ M Latrunculin A (middle column) or 2 mM Brefeldin A (right column) or nothing (control, left column), were submitted to a $\Delta C = -0.2 M$ hypotonic shock (t=0 min). Cells are considered dead if they contain large amounts of intracellular red fluorescence from the FM4-64 dye, which is the consequence of a rupture of the plasma membrane. Scale bar: 10 μ m. B) Survival rate for all conditions. Black: control (N=114); blue: 2 mM BFA (N=83); red: 25 μ M Latrunculin A (N=70). Data were pooled from two independent experiments and plotted as Kaplan-Meier survival curves. Error bars: standard error of the mean by the Greenwood formula. One star (*), $p \leq 0.05$, logrank test.

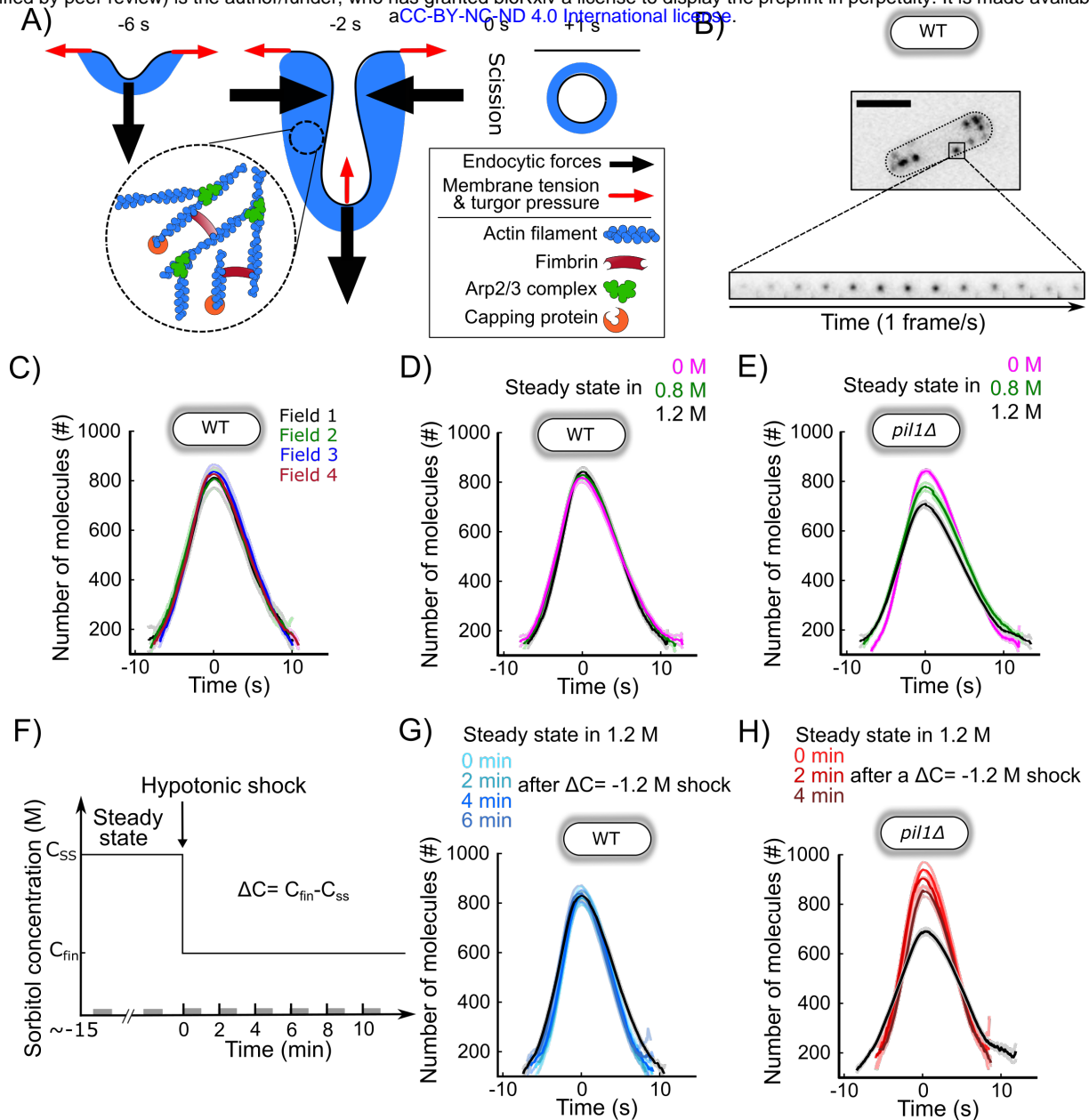


Figure 6: CME in walled cells is robust over a wide range of conditions. A) Schematic of the plasma membrane deformations and the main components of the actin machinery during CME. Fimbrin (Fim1p, red) crosslinks actin filaments (blue) present at endocytic sites and is used as a proxy to monitor the amount of actin assembled (Figure 6 – Supplement 1). B) Wild-type walled fission yeast cell expressing Fim1p-mEGFP (inverted contrast). Top: cell outlined with a dashed line; scale bar: 5 μm . Bottom: montage of a representative CME event. The interval between each frame is 1 s. C) The number of molecules of Fim1p-mEGFP detected, tracked and aligned with temporal super-resolution (Berro & Pollard, 2014) is highly reproducible between fields of view (one-way ANOVA on the number of molecules at time 0 s, $p=0.74$). Each curve with a dark color represents the average of several endocytic events from a different field of view of the same sample ($N \geq 64$), and the light colors are the 95% confidence intervals. For each average curve, the peak value corresponds to time 0 sec, when vesicle scission happens. D) Number of molecules of Fim1p-mEGFP in wild-type walled cells at steady state in media supplemented

with different sorbitol concentrations. There is no statistically significant difference in the number of molecules at time 0 s between the three conditions (one-way ANOVA, $p=0.29$). $N \geq 388$. E) Number of molecules of Fim1p-mEGFP in *pil1* Δ walled cells at steady state in media supplemented with different sorbitol concentrations ($N \geq 342$). The difference in the number of molecules at time 0 s between all pairs of conditions is statistically significant (one-way ANOVA, $p < 10^{-5}$). F) Timeline of the hypotonic shock experiments and notations. By convention, hypotonic shocks start at time 0 min and are defined by the difference in concentration of sorbitol in the steady state media before the shock (C_{SS}) and after the hypotonic shock (C_{fin}), $\Delta C = C_{fin} - C_{SS}$. Data for a given time point corresponds to endocytic events happening within 1 minute after this time point (e.g. the data at $t=0$ min correspond to endocytic events happening between 0 and 1 min after the shock). These time intervals are represented by gray bars on the time axis. G) Number of molecules of Fim1p-mEGFP for wild-type walled cells initially at steady state in 1.2 M sorbitol and after an acute osmotic shock of $\Delta C = -1.2$ M. There is no statistically significant difference in the number of molecules at time 0 s between the three conditions (one-way ANOVA, $p=0.95$). Black: steady state in 1.2 M sorbitol; light to dark blue in top panel: 0 min, 2 min, 4 min, and 6 min after the acute hypotonic shock ($N \geq 103$). H) Number of molecules of Fim1p-mEGFP in *pil1* Δ walled cells before and after an acute osmotic shock ($\Delta C = -1.2$ M). The difference in the number of molecules at time 0 s between all pairs of conditions is statistically significant (one-way ANOVA, $p < 0.03$) except between 0 min and 2 min after the shock (one-way ANOVA, $p=0.18$). Black: steady state in 1.2 M sorbitol before the hypotonic shock ($N=583$); light to dark red in top panel: 0 min, 2 min and 4 min after the acute hypotonic shock ($N \geq 145$). (C), (D), (E), (G) and (H): dark colors: average; light colors: average \pm 95% confidence interval. The number of molecules and speed versus time for each condition are plotted separately in Figure 6 – Supplement 2 (C), Figure 6 – Supplement 3 (D and G), Figure 6 – Supplement 4 (E and H). The numbers of endocytic events used in each curve are given in Supplemental Table 5 (C), Supplemental Table 6(D), Supplemental Tables 7 (E), Supplemental Table 8 (G), Supplemental Table 9 (H).

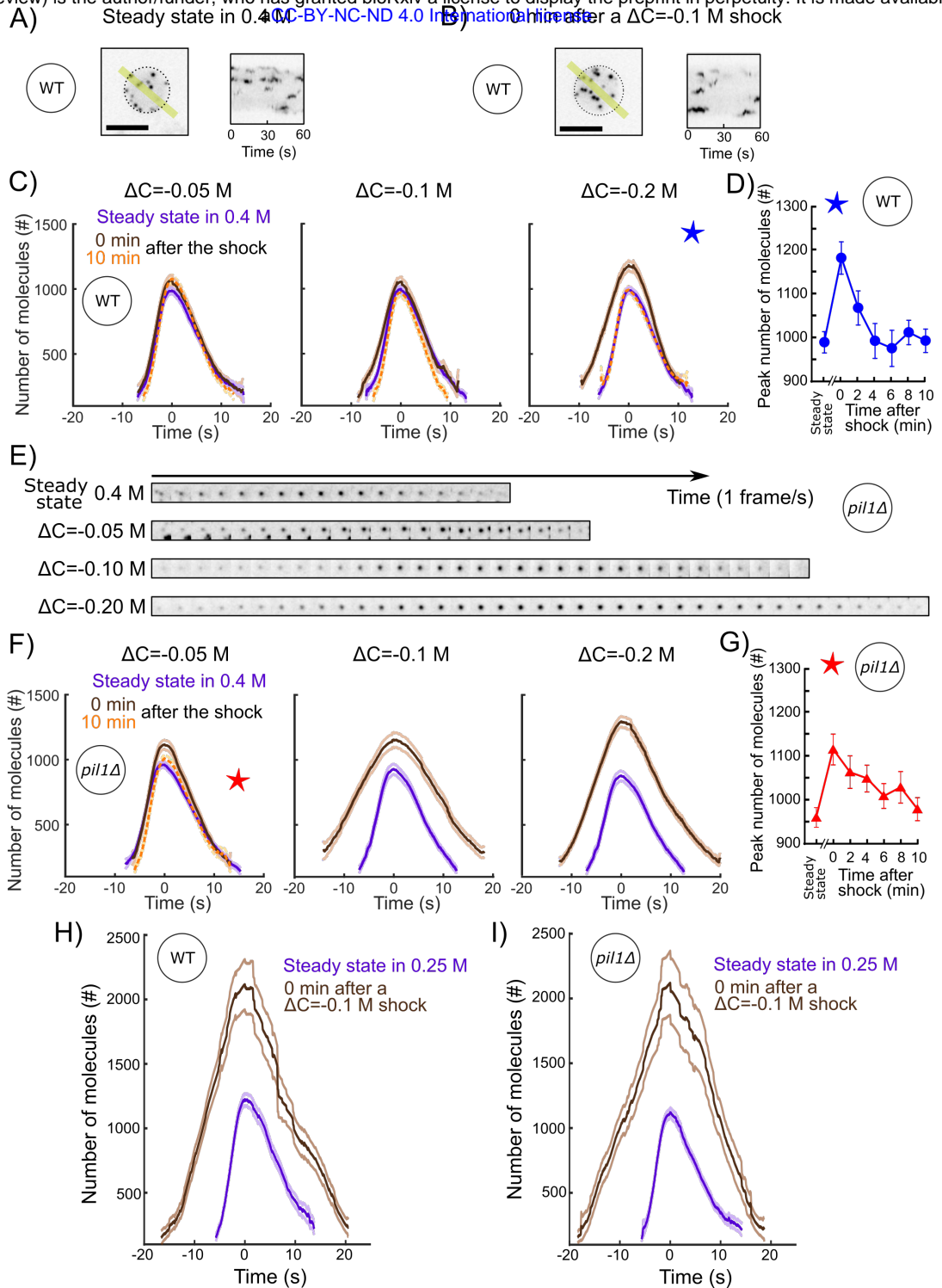










Figure 7: The actin endocytic machinery adapts to increases of membrane tension in protoplasts. A) and B) Representative wild-type protoplasts expressing Fim1-mEGFP (inverted contrast) at steady-state in 0.25 M sorbitol (A, left panel) and immediately after (0 min) an acute osmotic shock of $\Delta C = -0.1$ M (B, left panel). Right panels: kymographs of the fluorescence under the yellow lines in the left panels. Black dashed lines: protoplast outline. Scale bars: 5 μ m. C) and F) Number of Fim1p-mEGFP molecules in wild-type (C) and *pil1Δ* (F) protoplasts at steady-state in 0.4 M sorbitol (purple), 0 min (brown) and 10 min (orange) after an hypotonic shock of $\Delta C = -0.05$ M (left panels), $\Delta C = -0.1$ M (middle panels) and $\Delta C = -0.2$ M (right panels), $N \geq 95$.

Data for each condition are plotted separately in Figures 7 – Supplement 3 (wild type) and 7 – Supplement 4 (*pil1Δ*). The speeds of Fim1p-mEGFP for each condition are shown in Figures 7 – Supplement 5 (wild type) and 7 – Supplement 6 (*pil1Δ*). The numbers of endocytic events used in each curve are given in Supplemental Table 10. Note that the large majority of *pil1Δ* protoplasts were too damaged or dead 2 minutes after hypotonic shocks larger than or equal to $\Delta C = -0.1$ M to allow us to track enough endocytic events and produce a curve (Figures 2B, 2C and 2 – Supplement 1). In panel (C), the difference in the number of molecules at time 0 s at steady state and 0 min after the shock is statistically significant for all shocks (one-way ANOVA, $p < 0.03$) and the difference between steady-state and 10 min after the shock is not statistically significant (one-way ANOVA, $p > 0.2$; details in the data file for figure 7C). In panel (F), the difference at steady state and 0 min after the shock is statistically significant for all shocks (one-way ANOVA, $p < 10^{-5}$; details in the data file for figure 5F). D) Temporal adaptation of the peak number of Fim1p-mEGFP in wild-type protoplasts initially at steady state in 0.4 M sorbitol and 0 to 10 min after a $\Delta C = -0.2$ M osmotic shock. The condition for this figure is the same as the condition with the blue star in (C). The difference between steady-state and 0 min or 2 min after shock is statistically significant (one-way ANOVA, $p < 10^{-3}$; details in the data file for figure 7D). The difference between steady-state and 4 min, 6 min, 8 min and 10 min after shock is not statistically significant (one-way ANOVA, $p > 0.2$; details in the data file for figure 7D). E) Montage of representative endocytic events (Fim1-mEGFP, inverted contrast) in *pil1Δ* protoplasts (1 frame per second) at steady state in 0.4 M sorbitol (first row) and immediately after (0 min) a hypotonic shocks of $\Delta C = -0.05$ M (second row), $\Delta C = -0.10$ M (third row) and $\Delta C = -0.20$ M (fourth row). G) Temporal adaptation of the peak number of Fim1p-mEGFP in *pil1Δ* protoplasts initially at steady state in 0.4 M sorbitol and 0 to 10 min after a $\Delta C = -0.05$ M shock. The condition in this figure is the same as the condition with the red star in (F). The difference between steady-state and 0 min, 2 min, 4 min, 6 min or 8 min after shock is statistically significant (one-way ANOVA, $p < 0.01$; details in the data file for figure 7F). The difference between steady-state and 10 min after shock is not statistically significant (one-way ANOVA, $p > 0.3$; details in the data file for figure 7F). (D) and (G) error bars are 95% confidence intervals. The numbers of endocytic events at each time point are given in Supplemental Table 11. H) and I) Number of molecules of Fim1p-mEGFP for wild-type (H) and *pil1Δ* (I) protoplasts at steady state in 0.25 M sorbitol (purple dashed) and immediately after (0 min) a hypotonic shock of $\Delta C = -0.1$ M (brown), $N \geq 67$. The difference in the number of molecules at time 0 s at steady state and 0 min after the shock is statistically significant for all conditions (one-way ANOVA, $p < 10^{-16}$). The speed data for each condition are plotted in Figure 7 – Supplement 7. The numbers of endocytic events used in each curve are given in Supplemental Table 12. The survival rates for the wild-type and *pil1Δ* protoplasts in these conditions are plotted in Figure 2D.

- A)  Endocytic pit with actin patch  Cell wall
-  Pil1p  Membrane tension
-  Exocytic vesicle  Exocytosis
-  Endocytic vesicle  Endocytosis

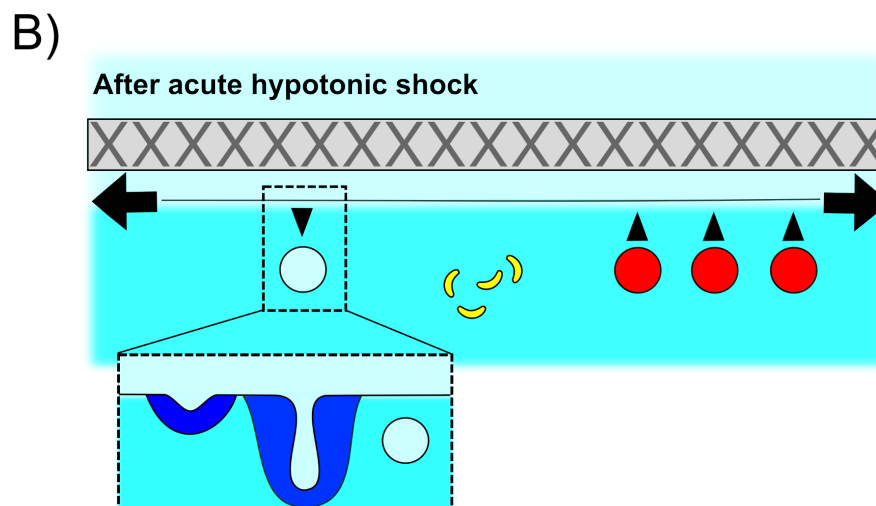
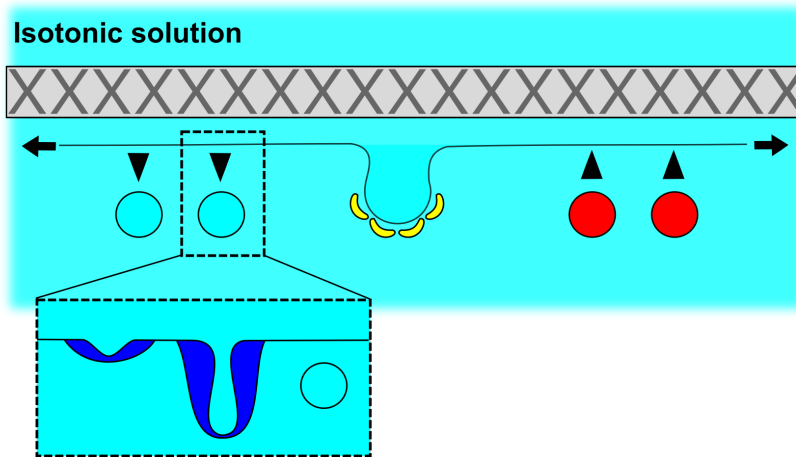


Figure 8: Schematic of the adaptation of fission yeast endocytosis, exocytosis and eisosome after acute hypotonic shock-induced increase in membrane tension. A) In an isotonic solution, endocytosis and exocytosis rates are largely balanced, and proteins including Pil1p are assembled at the plasma membrane to form eisosomes. Actin is recruited to endocytic sites to provide the forces needed to reshape the membrane under normal membrane tension. When present, cell wall makes fission yeast cell resistant to significant changes in the osmolarity of extracellular solution. B) Acute hypotonic shock results in an increase of membrane tension, which leads to a decrease of endocytosis rate, an increase in exocytosis rate, and a rapid disassembly of eisosomes, within ~2 minutes. The proteins of the actin machinery are recruited in larger amount to endocytic sites to provide larger forces for successful endocytosis under increased membrane tension. Failure of adaptation to the increase in membrane tension leads to membrane rupture and cell death in both protoplasts and walled cells.

bioRxiv preprint doi: <https://doi.org/10.1101/342030>; this version posted April 9, 2021. The copyright holder for this preprint (which was not certified by peer review) is the author/funder, who has granted bioRxiv a license to display the preprint in perpetuity. It is made available under aCC-BY-NC-ND 4.0 International license.

Supplemental Figures

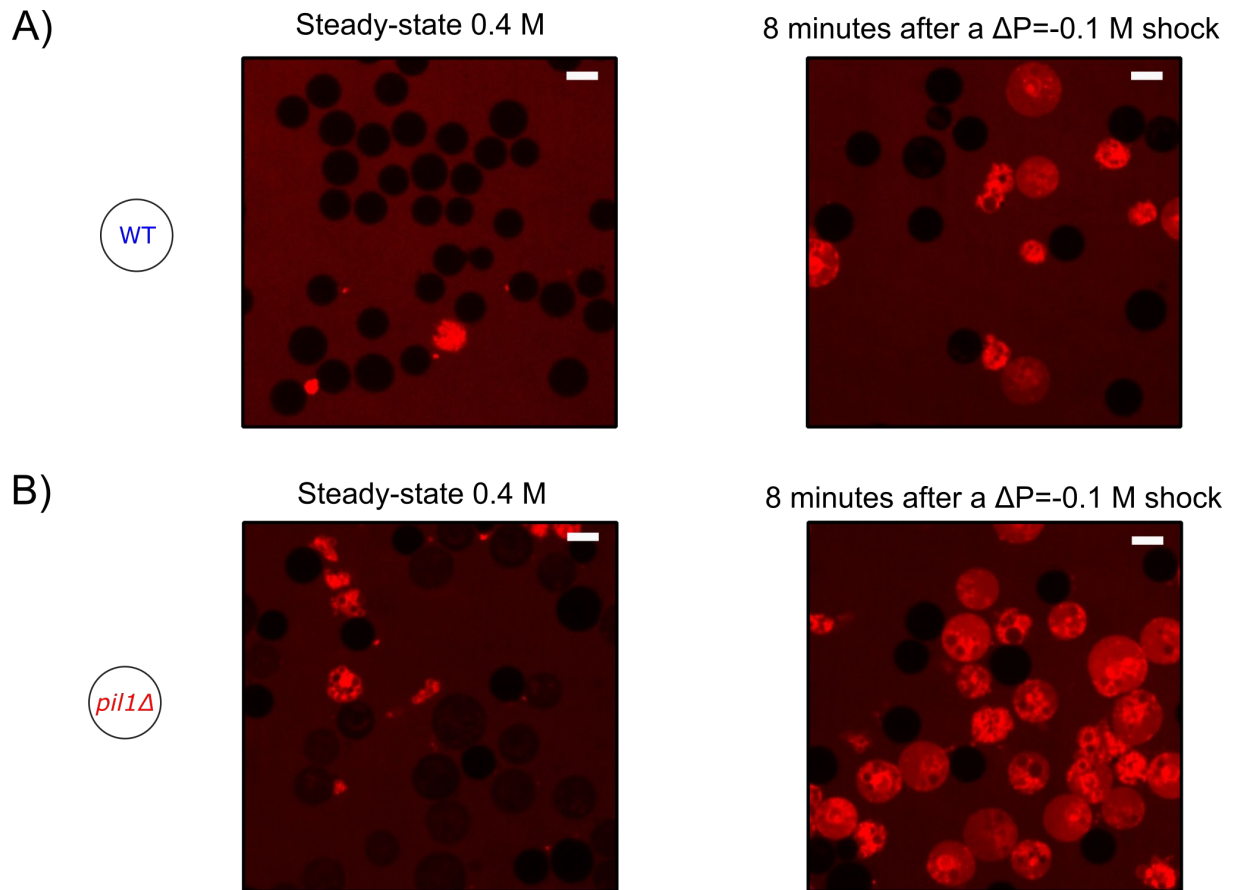


Figure 2 – Supplement 1: Typical fields of view of protoplasts at steady state in 0.4 M sorbitol and 8 minutes after a $\Delta C = -0.1$ M hypotonic shock. A) Wild-type. B) *pil1* Δ . Cells are considered alive if they do not contain any red fluorescence from the sulforhodamin B dye. Scale bar: 5 μ m.

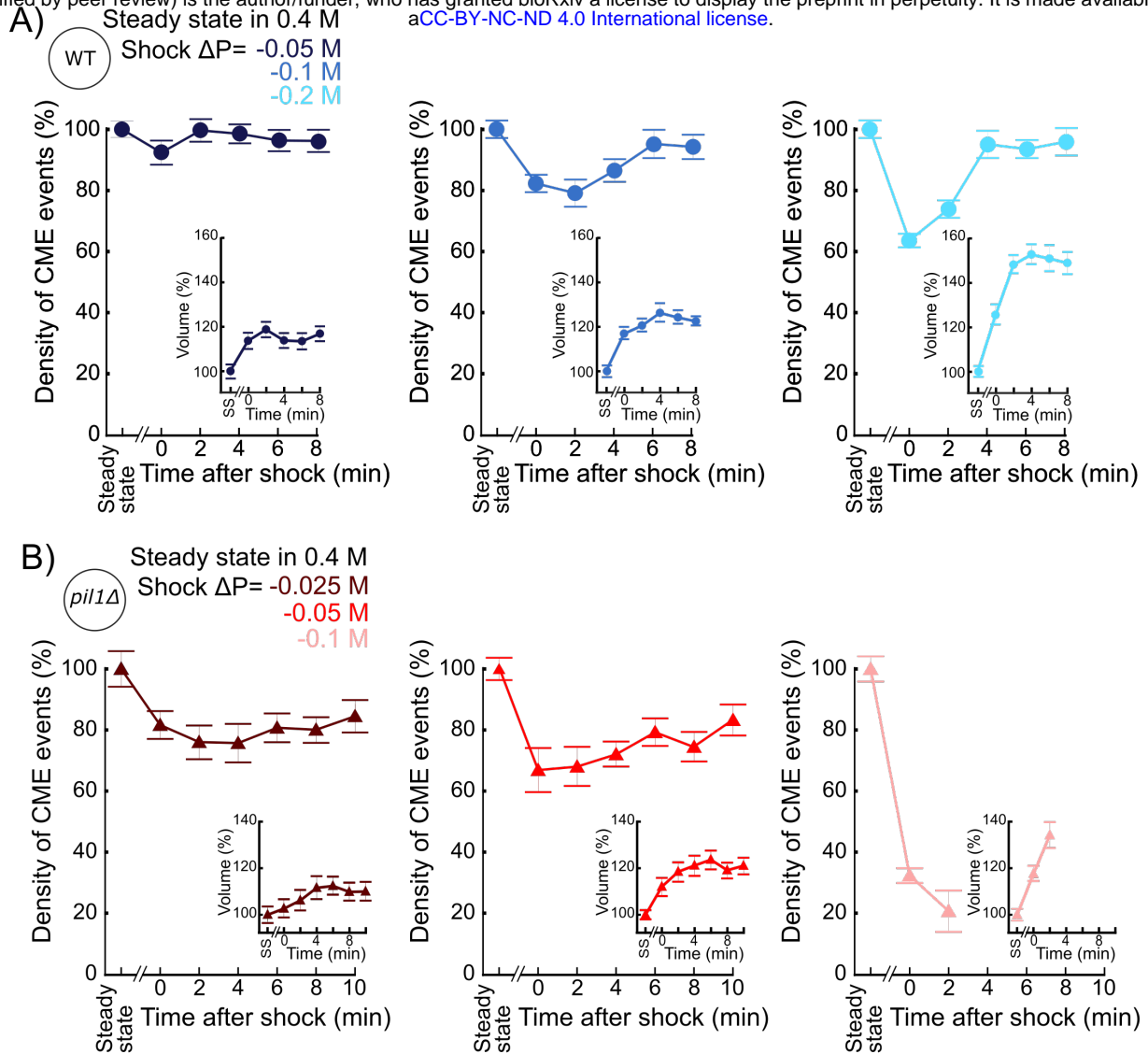


Figure 3 – Supplement 1: Separate plots for each condition shown in Figures 3A and 3B. A) Temporal evolution of density of endocytic events (average number of endocytic events at a given time in a cell divided by the cell length) in wild-type protoplasts initially at steady state in 0.4 M sorbitol and after an acute hypotonic shock of $\Delta C = -0.05$ M (dark blue, $N_{\text{cell}} \geq 102$), $\Delta C = -0.1$ M (blue, $N_{\text{cell}} \geq 54$) and $\Delta C = -0.2$ M (light blue, $N_{\text{cell}} \geq 83$). B) Same as (A) but with *pil1Δ* protoplasts and hypotonic shocks of $\Delta C = -0.025$ M (dark red, $N_{\text{cell}} \geq 70$), $\Delta C = -0.05$ M (red, $N_{\text{cell}} \geq 103$) and $\Delta C = -0.1$ M (light red, $N_{\text{cell}} \geq 78$). (A) and (B) insets: relative volume increase after the hypotonic shocks (the volume at steady state is used as a reference). The number of cells used for each condition and each time point is given in Supplemental Table 2. The number of cells measured in the insets are the same as in the main figures. (A) and (B): error bars are standard errors of the mean. The number of cells used for each condition and each time point is given in Supplemental Table 3.

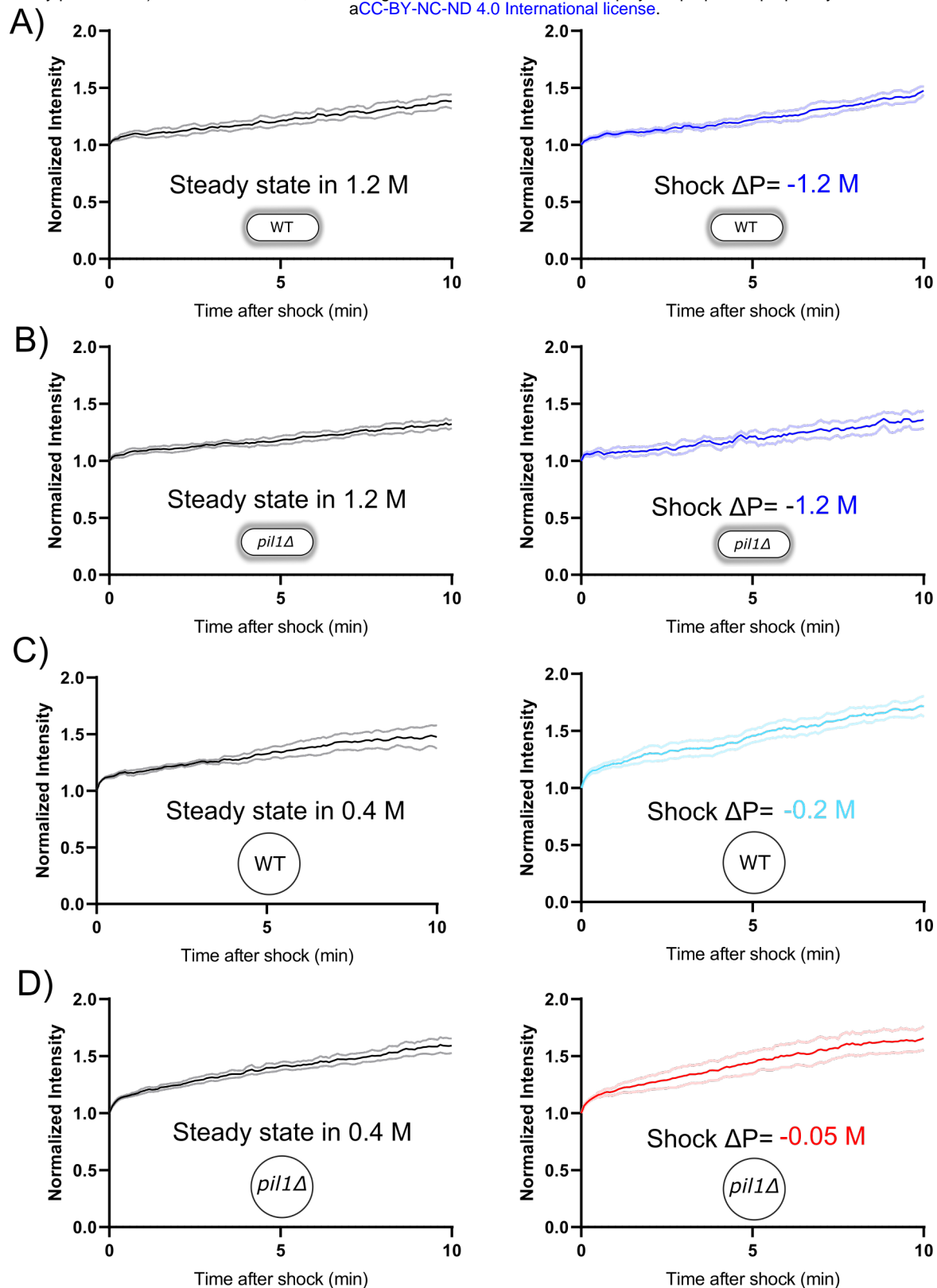


Figure 4 – Supplement 1: Separate plots for each condition in Figure 4. Rates of exocytosis at steady state and after hypotonic shocks. A) and B) The exocytic rate of wild-type walled cells is not changed after a $\Delta C = -1.2$ M acute hypotonic shock (black, before shock, $N_{\text{cells}} = 79$; blue, after shock, $N_{\text{cells}} = 68$; 3 replicates each). The exocytic rate of *pil1* Δ walled cells does not change significantly in the same conditions

(black, before shock, $N_{\text{cells}}=60$, blue, after shock, $N_{\text{cells}}=96$; 3 replicates each). All walled cells were at steady-state in 1.2 M sorbitol before time 0 min. C) and D) The exocytic rate of wild-type and *pil1* Δ protoplasts increases after a $\Delta C=-0.2$ M (black, before shock, $N_{\text{cells}}=20$; light blue, after shock, $N_{\text{cells}}=37$; 4 replicates each) and $\Delta C=-0.05$ M (black, before shock, $N_{\text{cells}}=44$; red, after shock, $N_{\text{cells}}=60$; 4 replicates each) acute hypotonic shocks, respectively. Before time 0 min, all protoplasts were at steady-state in 0.4 M sorbitol. (A)-(D) Dark color: mean; light color: standard error of the mean.

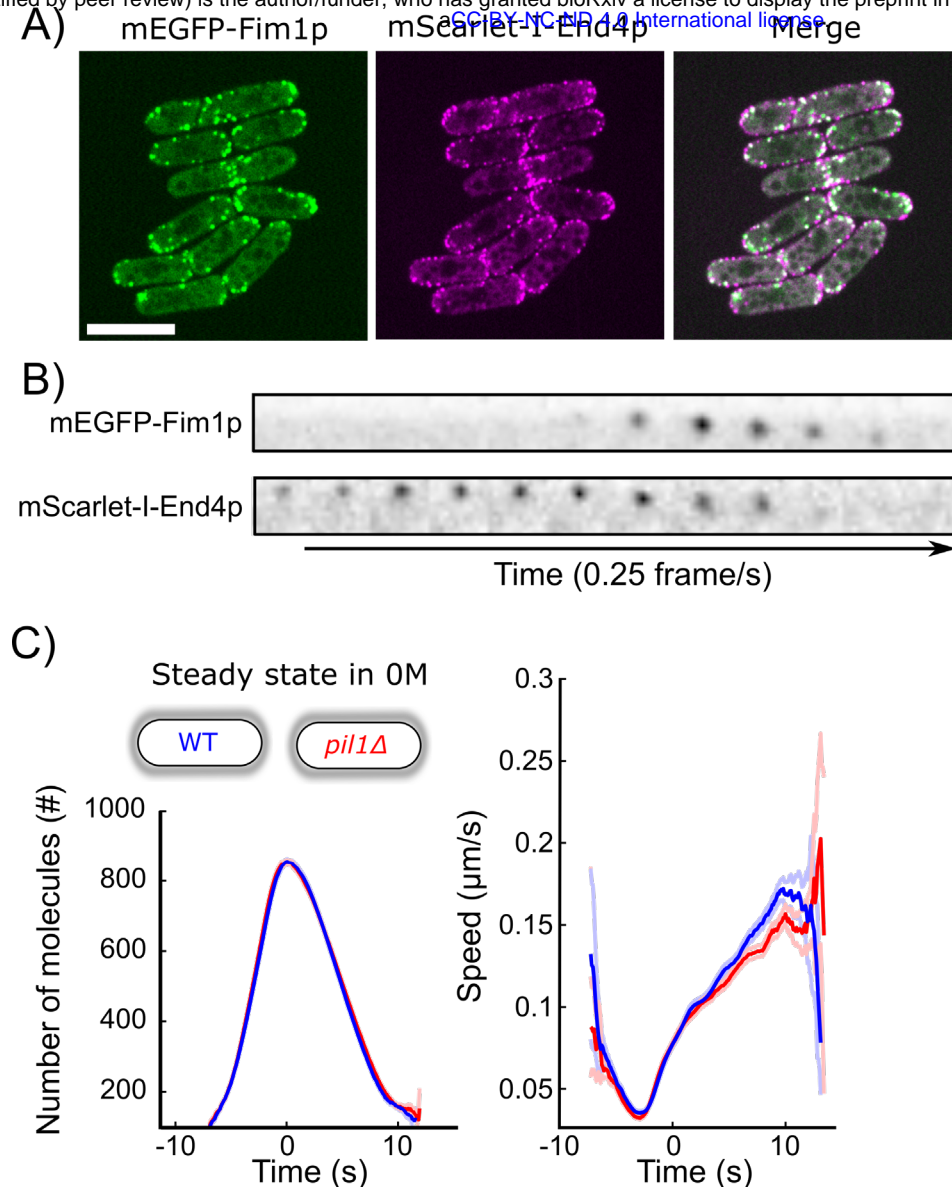


Figure 6 – Supplement 1: Fimbrin is a proxy for actin dynamics during CME in yeast and eisosomes do not participate in CME in wild-type walled cells.

A) Colocalization of Fimbrin (mEGFP-Fim1p, green) and End4 (mScarlet-I-End4p, red) during endocytosis. Significant overlapping of signals can be seen in the merged channel. B) Montage of a representative CME event tagged by both mEGFP-Fim1p (top-row) and mScarlet-I-End4p (bottom row). The interval between each frame is 4 s. C) The number of molecules (left panel) and speed (right panel) of Fim1p-mEGFP at CME sites in wild-type (blue, N=1773) and *pil1Δ* (red, N=1884) walled cells at steady state in EMM5S without sorbitol are identical (same data as Figures 6D and 6E). Dark colors: average, light colors: average \pm 95% confidence interval.

B)

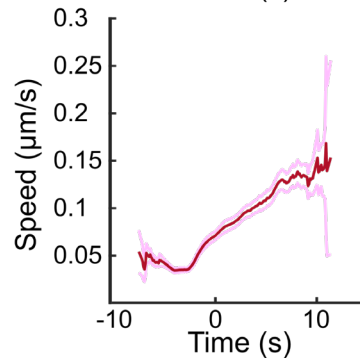
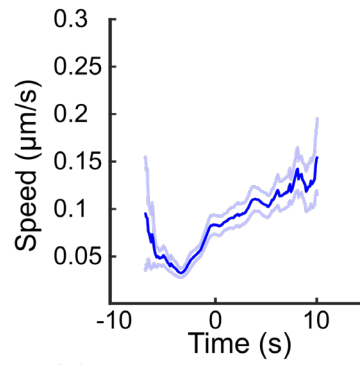
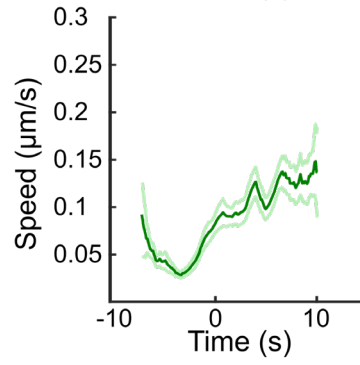
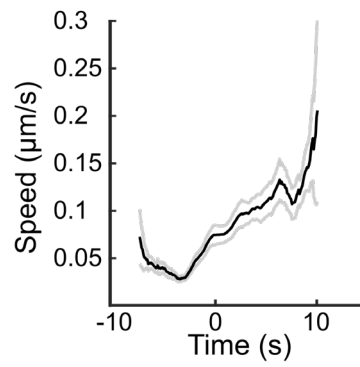
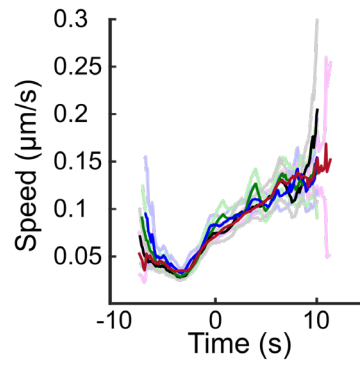
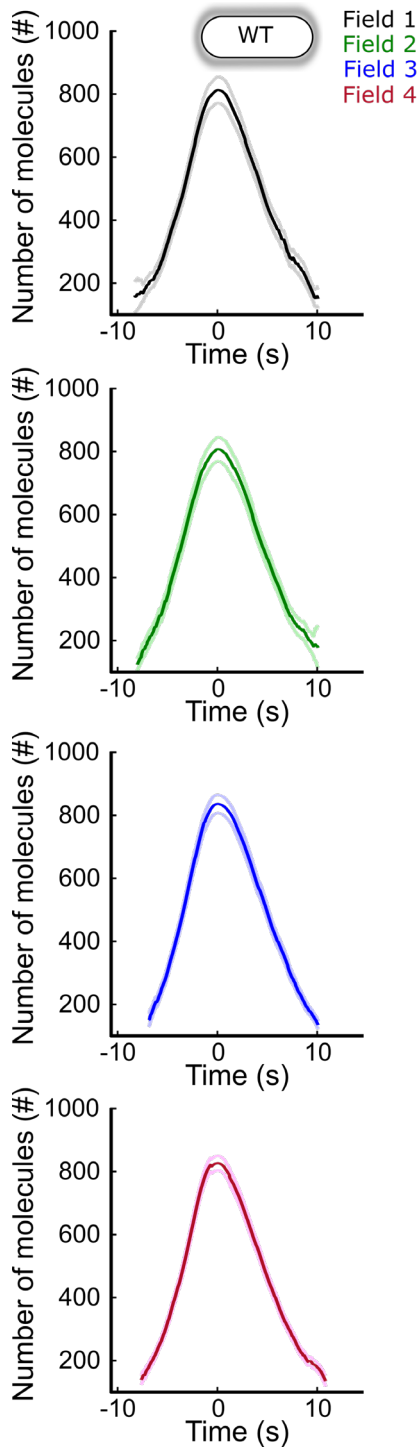
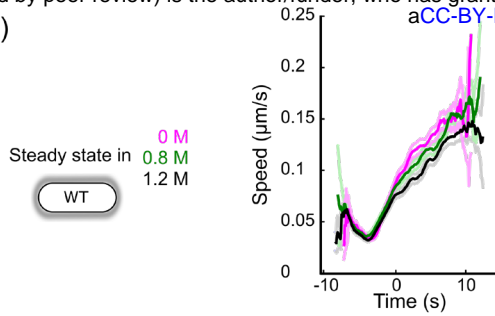
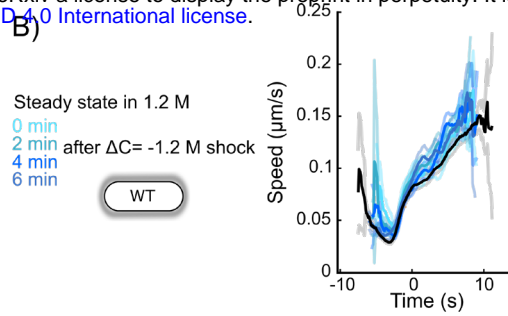


Figure 6 – Supplement 2: Speed data (A) and separate plots (B) for the data from each field of view in panel 1C. Each curve with a dark color represents the average of several endocytic events from a different field of view of the same sample ($N \geq 64$), and the light colors are the 95% confidence intervals. For each average curve, the peak value corresponds to time 0 sec, when vesicles scission happens. The numbers of endocytic events used in each curve are given in Supplemental Table 5.

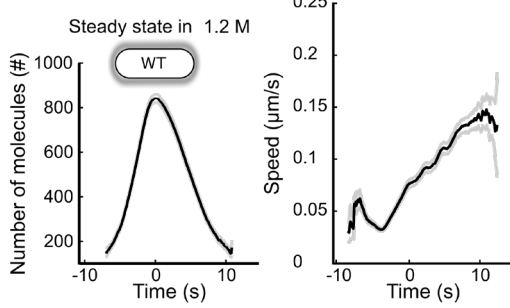
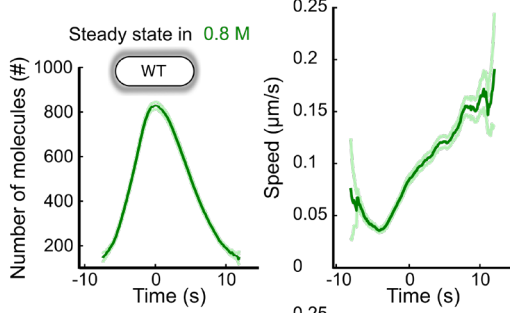
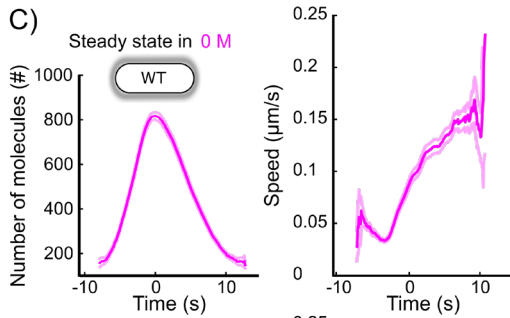
A)



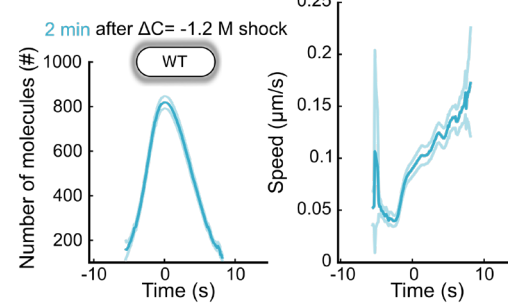
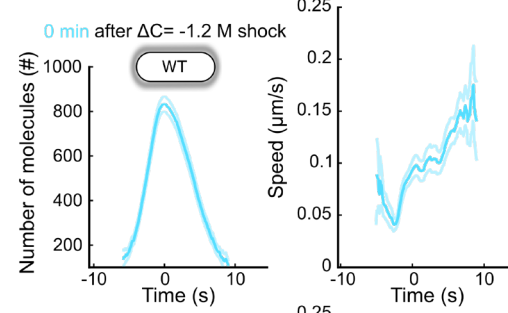
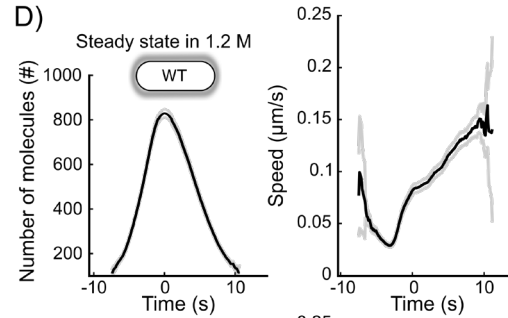
B)



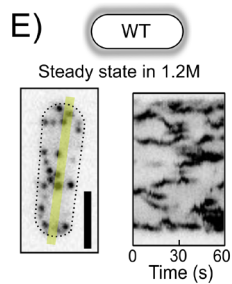
C)



D)



E)



F)

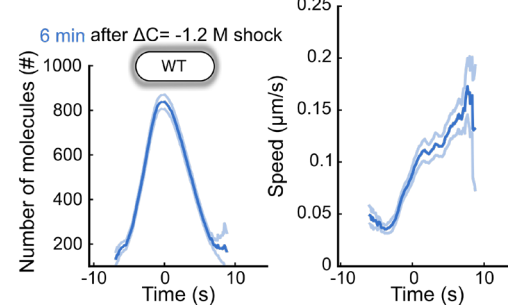
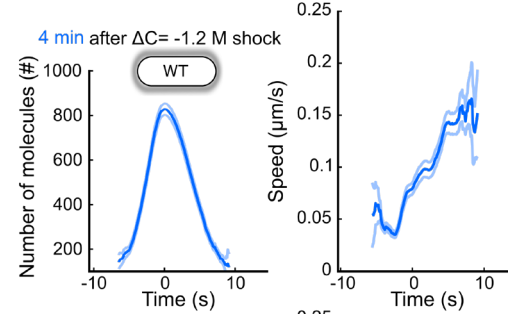
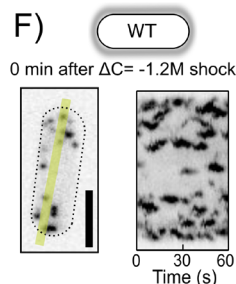


Figure 6 – Supplement 3: Representative endocytic events, speeds, and separate plots for each condition in Figures 6D and 6G.

A and B) Speeds corresponding to the data shown in Figures 6D (A) and 6G (B).

C) Number of molecules (left panel) and speed (right panel) of Fim1p-mEGFP in wild-type walled cells at steady state in media supplemented with different sorbitol concentrations ($N \geq 388$) (Figure 6D). The numbers of endocytic events used in each curve are given in Supplemental Table 6. D) Number of molecules (left panel) and speed (right panel) of Fim1p-mEGFP for wild-type walled cells initially at steady state in 1.2 M sorbitol and after an acute osmotic shock of $\Delta C = -1.2$ M. Black: steady state in 1.2 M sorbitol; light to dark blue (from top to bottom rows): 0 min, 2 min, 4 min, and 6 min after the acute hypotonic shock ($N \geq 103$) (Figure 6G). The numbers of endocytic events used in each curve are given in Supplemental Table 8. (C) and (D): dark colors: average; light colors: average \pm 95% confidence interval.

E) and F) Left panels: representative wild-type walled cells expressing Fim1p-mEGFP (inverted contrast) at steady state in 1.2 M sorbitol (E) and immediately (0 min) after an acute osmotic shock $\Delta C = -1.2$ M (F). Right panels: kymographs of the fluorescence under the yellow line in the left panels. Black dashed lines: outline of the cell. Scale bars for all panels: 5 μm .

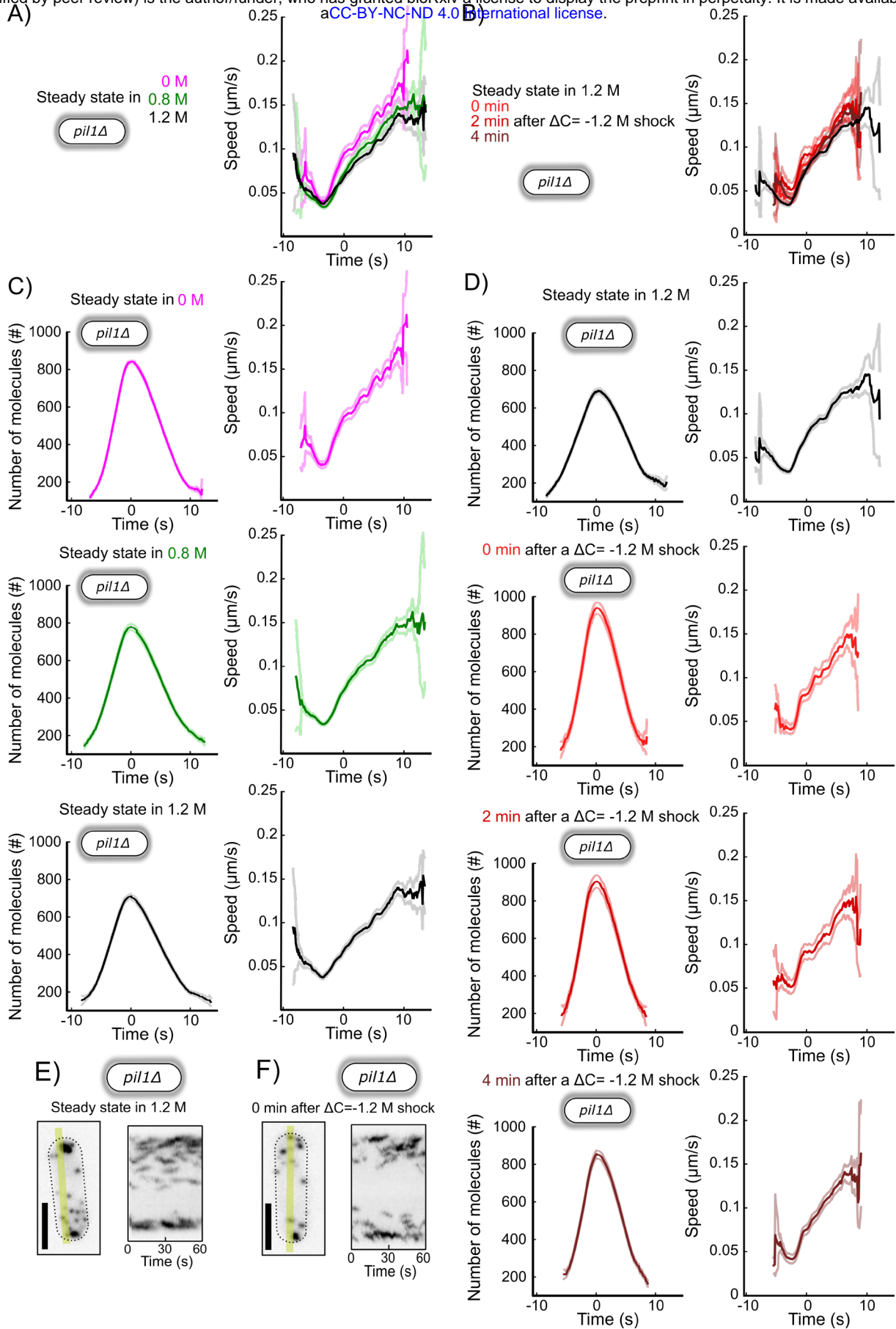


Figure 6 – Supplement 4: Representative endocytic events, speeds, and separate plots for each condition in Figures 6E and 6H.

A and B) Speeds corresponding to the data shown in Figures 6E (A) and 6H (B). C) Number of molecules (left panel) and speed (right panel) of Fim1p-mEGFP in *pil1* Δ walled cells at steady state in media supplemented with different sorbitol concentrations ($N \geq 342$) (Figure 6E). The numbers of endocytic events used in each curve are given in Supplemental Table 6. D) Number of molecules (left panel) and speed (right panel) of Fim1p-mEGFP for wild-type walled cells initially at steady state in 1.2 M sorbitol and after an acute osmotic shock of $\Delta C = -1.2$ M. Black: steady state in 1.2 M sorbitol; light to dark blue (from top to bottom rows): 0 min, 2 min and 4 min after the acute hypotonic shock ($N \geq 145$) (Figure 6H). The numbers of endocytic events used in each curve are given in Supplemental Table 8. (C) and (D): dark colors: average; light colors: average \pm 95% confidence interval.

E) and F) Left panels: representative *pil1* Δ walled cells expressing Fim1p-mEGFP (inverted contrast) at steady state in 1.2 M sorbitol (E) and immediately (0 min) after an acute osmotic shock $\Delta C = -1.2$ M (F). Right panels: kymographs of the fluorescence under the yellow line in the left panels. Black dashed lines: outline of the cell. Scale bars for all panels: 5 μ m.

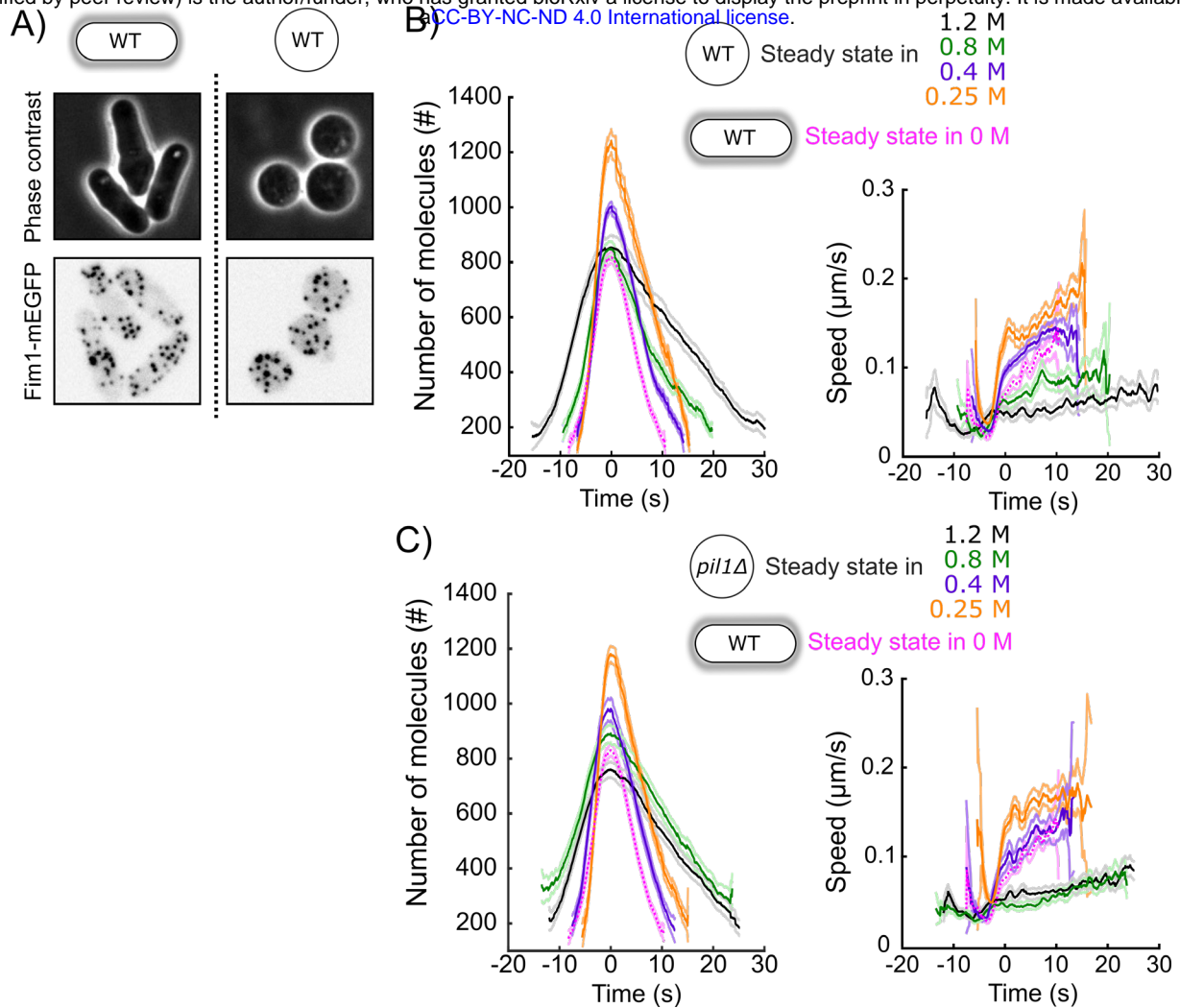


Figure 7 – Supplement 1: CME in protoplasts at steady-state in different sorbitol concentrations. A) Representative walled yeast cells (left column) and protoplasts (right column) at steady state in 1.2 M sorbitol. Top panels: phase contrast; middle panels: cells expressing Fim1-mEGFP (inverted contrast). B) and C) Number of molecules (left panels) and speed (right panels) of Fim1p-mEGFP for wild-type (B) and *pil1Δ* (C) protoplasts at steady state in different sorbitol concentrations. Orange: 0.25 M; purple: 0; green: 0.8 M; black: 1.2 M. Dark colors: average; light colors: average \pm 95% confidence interval ($N \geq 143$). Fuchsia dotted curves: wild-type walled cells at steady state in 0 M sorbitol. Data for each condition are plotted separately in Figure 7 – Supplement 2. The numbers of endocytic events used in each curve are given in Supplemental Table 13.

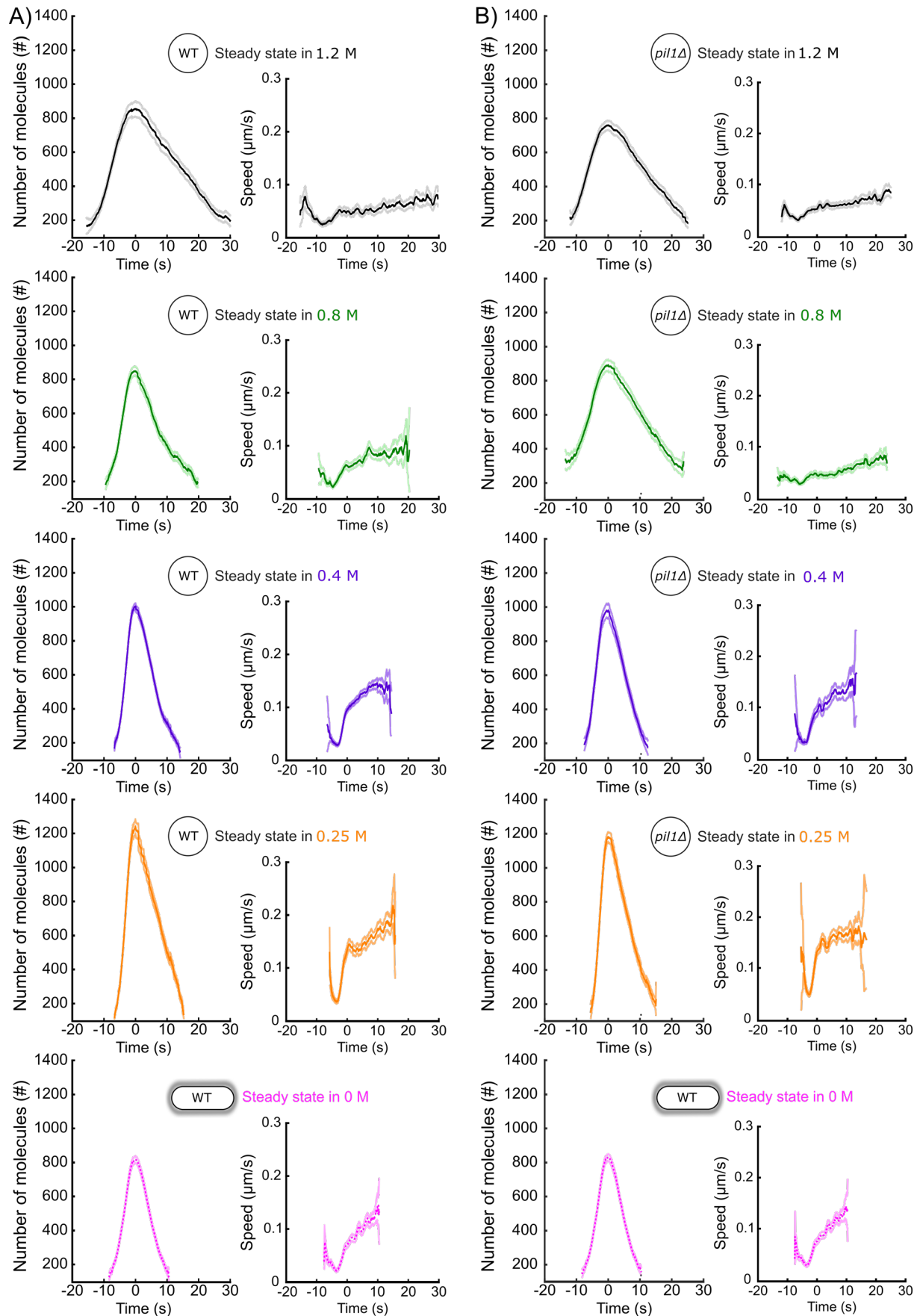


Figure 7 – Supplement 2: Separate plots for each condition in Figure 7 – Supplement 1. A) and B) Number of molecules (left panels) and speed (right panels) of Fim1p-mEGFP for wild-type (A) and *pil1Δ* (B) protoplasts at steady state in different sorbitol concentrations. Orange: 0.25 M; purple: 0; green: 0.8 M; black: 1.2 M. Dark colors: average; light colors: average +/- 95% confidence interval (N≥143). Fuschia dotted curves: walled cells at steady state in 0 M sorbitol (same as Figures 6D and 6E). The numbers of endocytic events used in each curve are given in Supplemental Table 13.

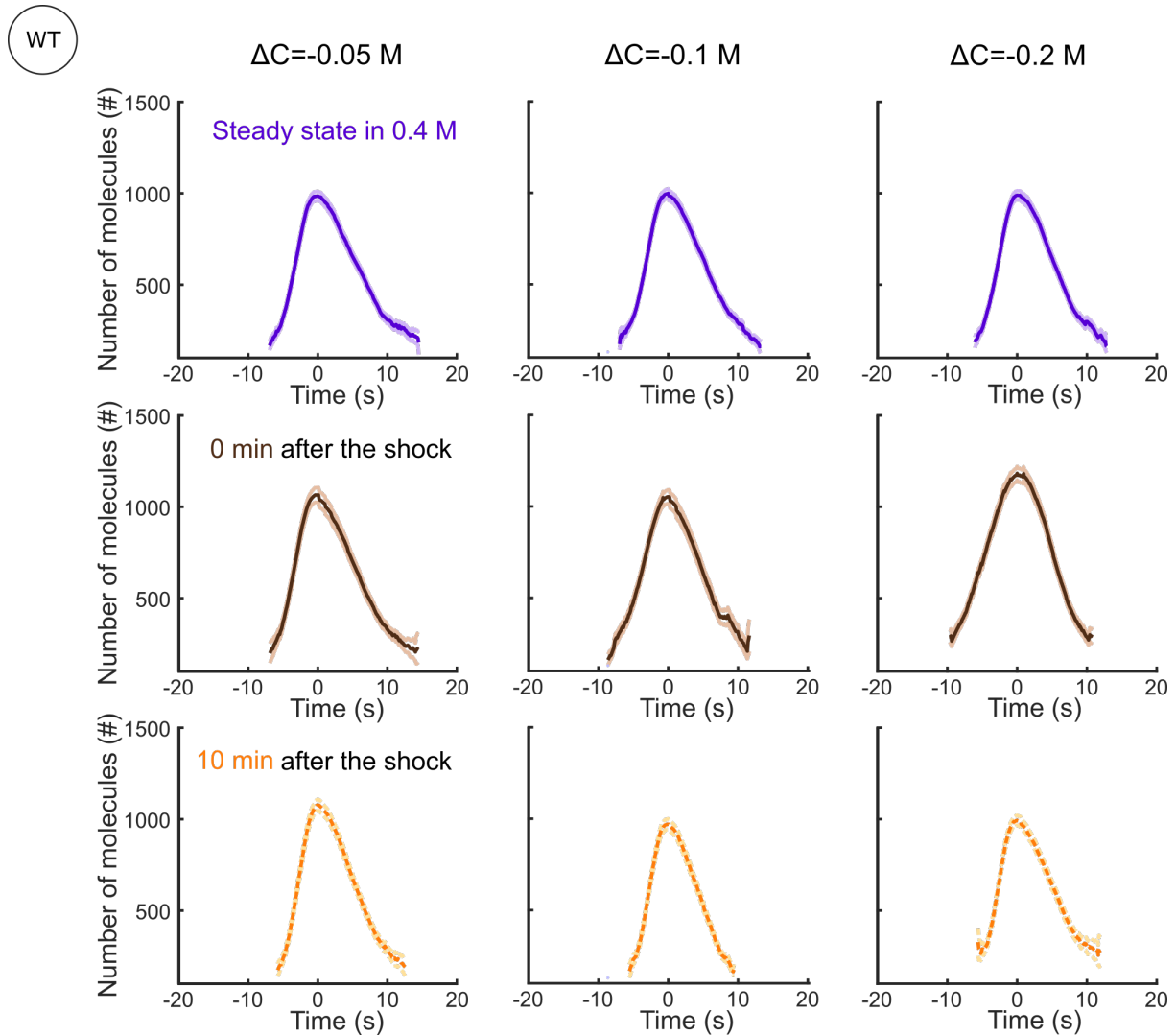


Figure 7 – Supplement 3: Separate plots for each condition shown in Figure 7C. Number of Fim1p-mEGFP molecules in wild-type protoplasts at steady-state in 0.4 M sorbitol (purple), 0 min (brown) and 10 min (orange) after an hypotonic shock of $\Delta C = -0.05$ M (left panels), $\Delta C = -0.1$ M (middle panels) and $\Delta C = -0.2$ M (right panels), $N \geq 95$. The speeds of Fim1p-mEGFP for each condition are shown in Figure 7 – Supplement 5. The numbers of endocytic events used in each curve are given in Supplemental Table 10. Dark colors: average, light colors: average \pm 95% confidence interval.

pil1Δ

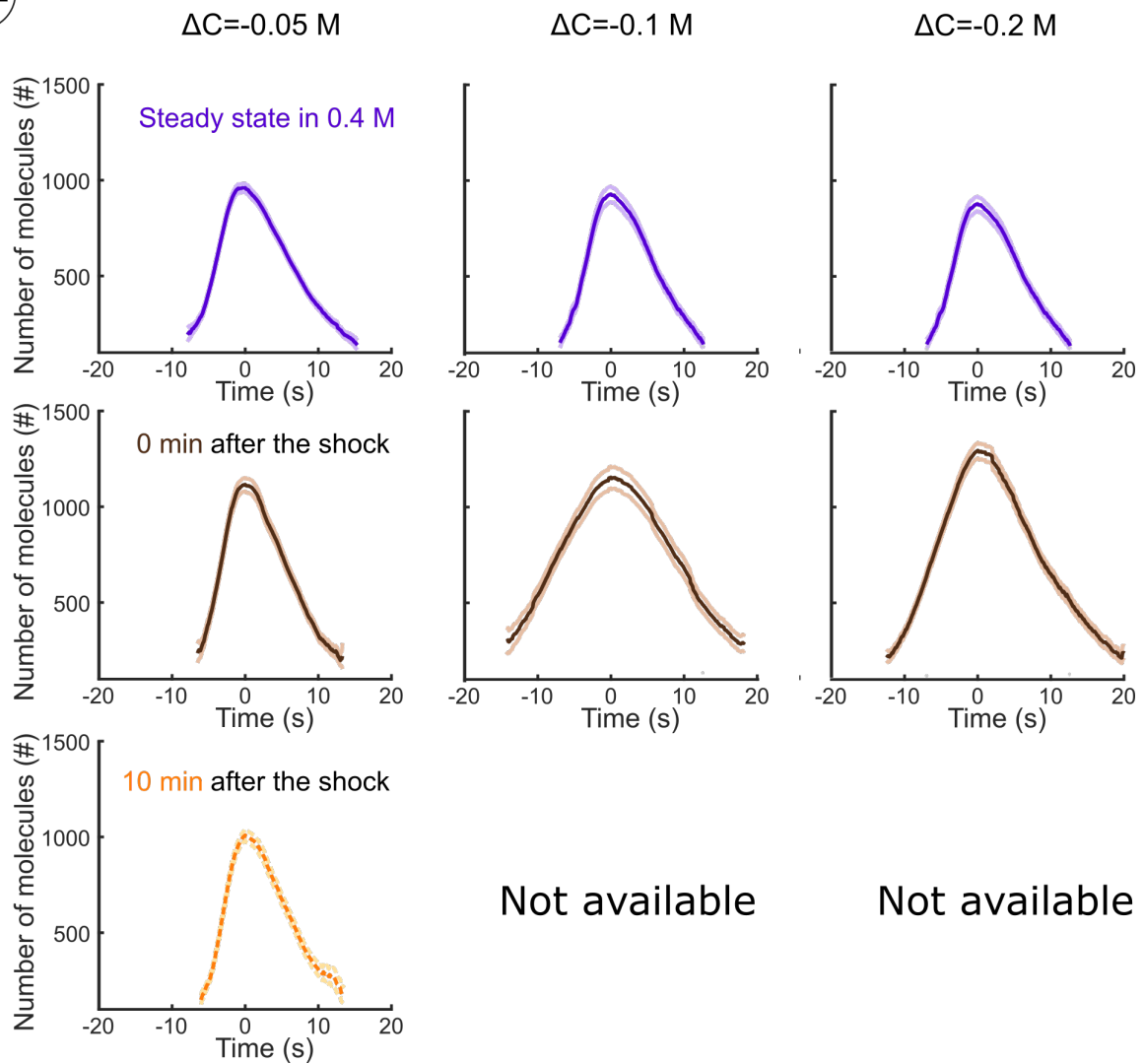
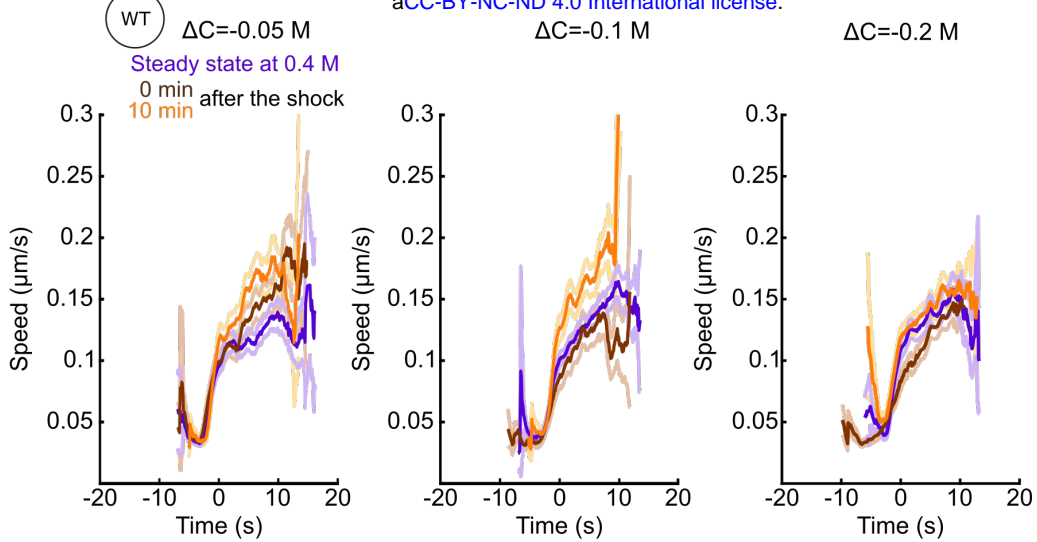


Figure 7 – Supplement 4: Separate plots for each condition shown in Figure 7F. Number of Fim1p-mEGFP molecules in *pil1Δ* protoplasts at steady-state in 0.4 M sorbitol (purple), 0 min (brown) and 10 min (orange) after an hypotonic shock of $\Delta C = -0.05$ M (left panels), $\Delta C = -0.1$ M (middle panels) and $\Delta C = -0.2$ M (right panels), $N \geq 95$. The speeds of Fim1p-mEGFP for each condition are shown in Figure 7 – Supplement 6. The numbers of endocytic events used in each curve are given in Supplemental Table 10. Note that the large majority of *pil1Δ* protoplasts were too damaged or dead 2 minutes after hypotonic shocks larger than or equal to $\Delta C = -0.1$ M to allow us to track enough endocytic events and produce a curve (Figures 2B, 2C and 2 – Supplement 1). Dark colors: average, light colors: average \pm 95% confidence interval.

A)



B)

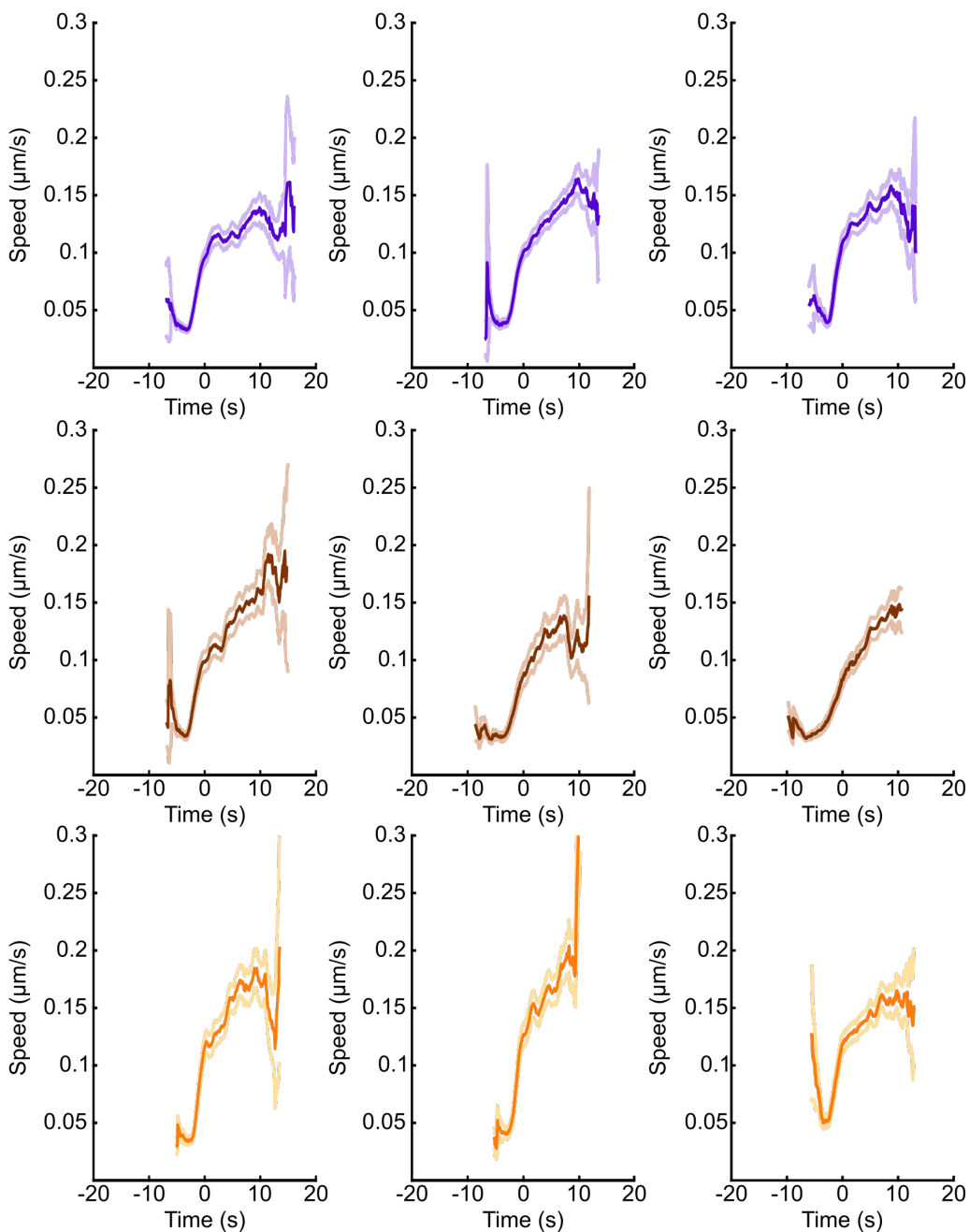
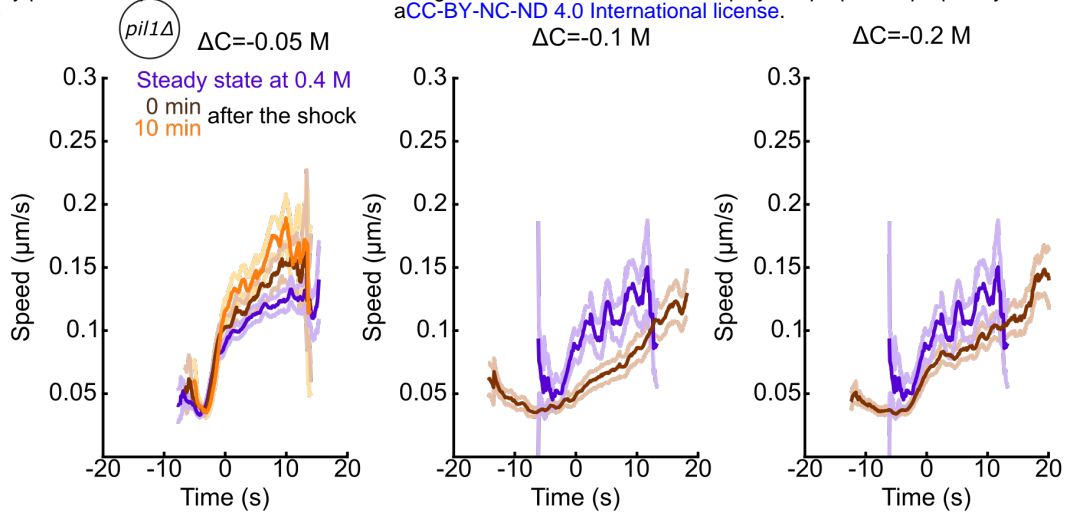


Figure 7 – Supplement 5: Speeds and separate plots for each condition shown in Figure 7C A) Speed of Fim1p-mEGFP in wild-type protoplasts at steady-state in 0.4 M sorbitol (purple), 0 min (brown) and 10 min (orange) after an hypotonic shock of $\Delta C = -0.05$ M (left panels), $\Delta C = -0.1$ M (middle panels) and $\Delta C = -0.2$ M (right panels). B) Separate plots for each condition shown in panel A. (A and B) The same endocytic events as the ones used in Figure 7C have been used to generate these plots. The numbers of endocytic events used in each curve are given in Supplemental Table 10. Dark colors: average, light colors: average \pm 95% confidence interval.

A)



B)

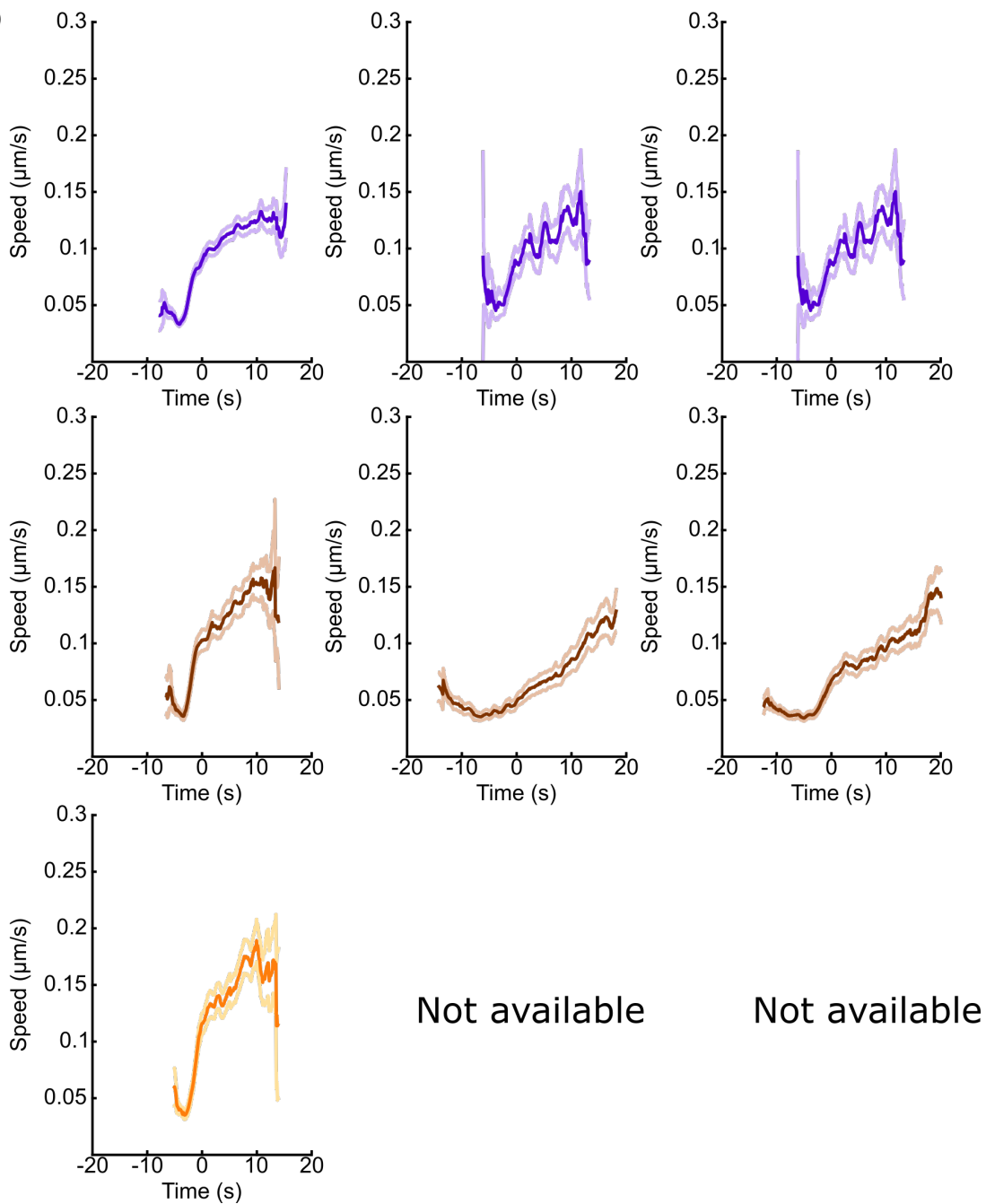


Figure 7 – Supplement 6: Speeds and separate plots for each condition shown in Figure 7F A) Speed of Fim1p-mEGFP in *pil1Δ* protoplasts at steady-state in 0.4 M sorbitol (purple), 0 min (brown) and 10 min (orange) after an hypotonic shock of $\Delta C = -0.05$ M (left panels), $\Delta C = -0.1$ M (middle panels) and $\Delta C = -0.2$ M (right panels). B) Separate plots for each condition shown in panel A. (A and B) The same endocytic events as the ones used in Figure 7F have been used to generate these plots. The numbers of endocytic events used in each curve are given in Supplemental Table 10. Dark colors: average, light colors: average \pm 95% confidence interval.

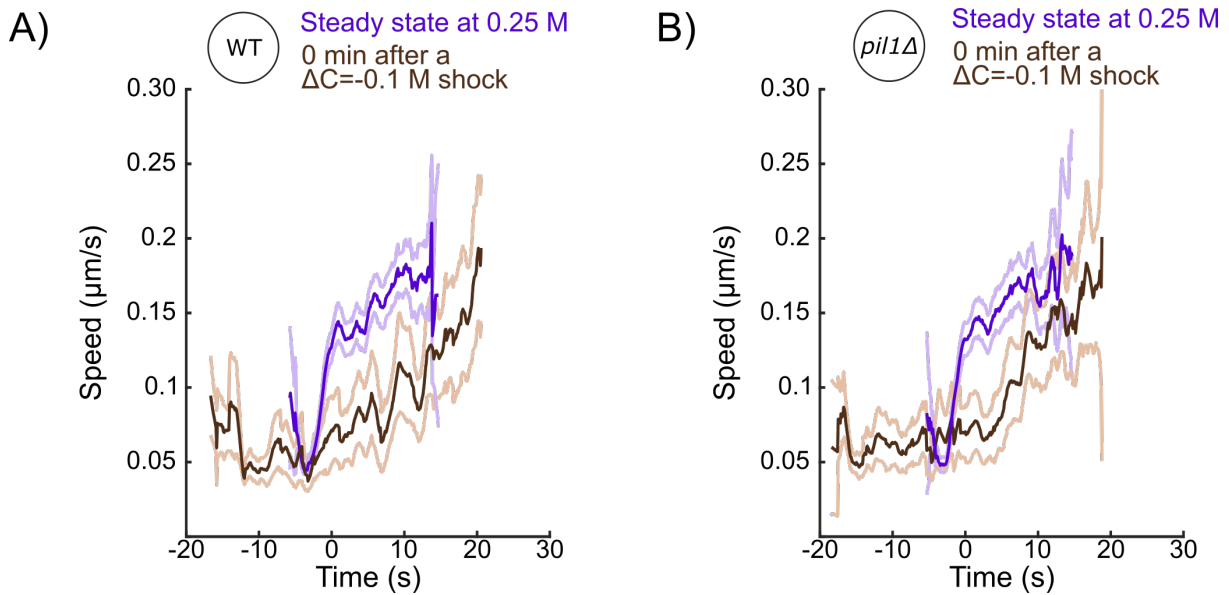


Figure 7 – Supplement 7: Speed of Fim1p-mEGFP at CME sites for wild-type (A) and *pil1* Δ (B) protoplasts at steady-state in 0.25 M sorbitol (purple) and immediately (0 min) after (brown) a hypotonic shock of $\Delta\text{C}=-0.1$ M. The same endocytic events as the ones used in Figures 7H (A) and 7I (B) have been used to generate these plots. The numbers of endocytic events used in each curve are given in Supplemental Table 12. Dark colors: average, light colors: average \pm 95% confidence interval.

bioRxiv preprint doi: <https://doi.org/10.1101/342030>; this version posted April 9, 2021. The copyright holder for this preprint (which was not certified by peer review) is the author/funder, who has granted bioRxiv a license to display the preprint in perpetuity. It is made available under a [CC-BY-NC-ND 4.0 International license](#).

Supplemental tables

Supplemental Table 1: Yeast strains

Strain	Genotype	Mating type
SpJB57	fim1-mEGFP-NatMX6 ade6-M216 his3- Δ 1 leu1-32 ura4- Δ 18	h+
SpJB204	pil1-mEGFP-kanMX6 ade6-M216 his3- Δ 1 leu1-32 ura4- Δ 18	h-
SpJB234	pil1 Δ fim1-mEGFP-NatMX6 ade6-M216 his3- Δ 1 leu1-32 ura4- Δ 18	h-
SpJB566	mScarlet-I-end4 mEGFP-fim1 fex1 Δ fex2 Δ ade6-M216 his3-D1 leu1-32 ura4-D18	h-

Supplemental Table 2: Number of cells used to generate Figures 3A and 3B

$\Delta C = -0.025M$

Time point	Number of cells WT cells	Number of cells <i>pil1</i> Δ cells
Steady state in 0.4M	\emptyset	99
0 min after $\Delta C = -0.025 M$	\emptyset	100
2 min after $\Delta C = -0.025 M$	\emptyset	71
4 min after $\Delta C = -0.025 M$	\emptyset	70
6 min after $\Delta C = -0.025 M$	\emptyset	98
8 min after $\Delta C = -0.025 M$	\emptyset	118
10 min after $\Delta C = -0.025 M$	\emptyset	96

$\Delta C = -0.05M$

Time point	Number of cells WT cells	Number of cells <i>pil1</i> Δ cells
Steady state in 0.4M	172	263
0 min after $\Delta C = -0.05 M$	102	106
2 min after $\Delta C = -0.05 M$	117	111
4 min after $\Delta C = -0.05 M$	114	106
6 min after $\Delta C = -0.05 M$	113	103
8 min after $\Delta C = -0.05 M$	124	123
10 min after $\Delta C = -0.05 M$	\emptyset	104

$\Delta C = -0.1M$

Time point	Number of cells WT cells	Number of cells <i>pil1</i> Δ cells
Steady state 0.4M	127	151

0 min after $\Delta C = -0.1$ M	62	125
2 min after $\Delta C = -0.1$ M	70	78
4 min after $\Delta C = -0.1$ M	78	\emptyset
6 min after $\Delta C = -0.1$ M	62	\emptyset
8 min after $\Delta C = -0.1$ M	54	\emptyset

$\Delta C = -0.2$ M

Time point	Number of cells WT cells	Number of cells <i>pil1</i> Δ cells
Steady state 0.4M	146	\emptyset
0 min after $\Delta C = -0.2$ M	149	\emptyset
2 min after $\Delta C = -0.2$ M	158	\emptyset
4 min after $\Delta C = -0.2$ M	83	\emptyset
6 min after $\Delta C = -0.2$ M	107	\emptyset
8 min after $\Delta C = -0.2$ M	83	\emptyset

Supplemental Table 3: Number of cells used to generate Figure 3C

Sorbitol Concentration	Number of cells WT cells	Number of cells <i>pil1</i> Δ cells
Steady state in 0 M	240	188
Steady state in 0.8 M	103	105
Steady state in 1.2 M	159	183
Steady state in 2 M	161	80

Supplemental Table 4: Number of cells used to generate Figure 3D

Time point	Number of cells WT cells	Number of cells <i>pil1</i> Δ cells
Steady state 1.2M	62	119
0 min after $\Delta C = -1.2$ M	82	69
2 min after $\Delta C = -1.2$ M	77	44
4 min after $\Delta C = -1.2$ M	67	67
6 min after $\Delta C = -1.2$ M	66	\emptyset

Supplemental Table 5: Number of endocytic events used to generate Figures 6C and 6 – Supplement 2A

Field of view	Number of tracks
---------------	------------------

Field 1	64
Field 2	79
Field 3	91
Field 4	202

Supplemental Table 6: Number of endocytic events used to generate Figure 6D

Sorbitol concentration	Number of tracks
0 M	388
0.8 M	454
1.2 M	451

Supplemental Table 7: Number of endocytic events used to generate Figure 6E

Sorbitol concentration	Number of tracks
0 M	342
0.8 M	516
1.2 M	514

Supplemental Table 8: Number of endocytic events used to generate Figure 6G

Time point	Number of tracks
Steady state	354
0 min	103
2 min	169
4 min	190
6 min	153

Supplemental Table 9: Number of endocytic events used to generate Figure 6H

Time point	Number of tracks
Steady state	583
0 min	176
2 min	145
4 min	326

Supplemental Table 10: Number of endocytic events used to generate Figures 7C and 7F

$\Delta C = -0.05M$

Time point	Number of tracks WT cells	Number of tracks <i>pil1</i> Δ cells
Steady state in 0.4M	279	429
0 min after $\Delta C = -0.05M$	193	183
10 min after $\Delta C = -0.05M$	182	206

$\Delta C = -0.1M$

Time point	Number of tracks WT cells	Number of tracks <i>pil1</i> Δ cells
Steady state in 0.4M	413	95
0 min after $\Delta C = -0.1M$	190	215
10 min after $\Delta C = -0.1M$	186	\emptyset

$\Delta C = -0.2M$

Time point	Number of tracks WT cells	Number of tracks <i>pil1</i> Δ cells
Steady state in 0.4M	269	95
0 min after $\Delta C = -0.2M$	396	373
10 min after $\Delta C = -0.2M$	309	\emptyset

Supplemental Table 11: Number of endocytic events used to generate Figures 7D and N7G

Time point	Number of tracks WT cells
Steady state in 0.4M	269
0 min after $\Delta C = -0.2M$	396
2 min after $\Delta C = -0.2M$	124
4 min after $\Delta C = -0.2M$	127
6 min after $\Delta C = -0.2M$	178
8 min after $\Delta C = -0.2M$	255
10 min after $\Delta C = -0.2M$	309

Time point	Number of tracks <i>pil1Δ</i> cells
Steady state in 0.4M	429
0 min after $\Delta C = -0.05M$	183
2 min after $\Delta C = -0.05M$	188
4 min after $\Delta C = -0.05M$	162
6 min after $\Delta C = -0.05M$	193
8 min after $\Delta C = -0.05M$	197
10 min after $\Delta C = -0.05M$	206

Supplemental Table 12: Number of endocytic events used to generate Figures 7H and 7I

Time point	Number of tracks WT cells	Number of tracks <i>pil1Δ</i> cells
Steady state in 0.25M	226	182
0 min after $\Delta C = -0.1 M$	75	67

Supplemental Table 13: Number of endocytic events used to generate Figures 7 – Supplement 1B and 7 – Supplement 1C

Sorbitol concentration	Number of tracks WT cells	Number of tracks <i>pil1Δ</i> cells
Protoplasts in 1.2 M	143	203
Protoplasts in 0.8 M	151	184
Protoplasts in 0.4 M	682	166
Protoplasts in 0.25 M	395	370
WT walled cells in 0M	234	300